WHITE PAPER

JANUARY 2022

DECARBONIZING BULK CARRIERS WITH HYDROGEN FUEL CELLS AND WIND-ASSISTED PROPULSION: A MODELED CASE STUDY ANALYSIS

Bryan Comer, PhD and Elise Georgeff
International Council on Clean Transportation

Douglas Stolz, PhD
Cross Product Atmospheric LLC

Xiaoli Mao and Liudmila Osipova, PhD
International Council on Clean Transportation

www.theicct.org

communications@theicct.org

twitter @theicct

icct
THE INTERNATIONAL COUNCIL ON CLEAN TRANSPORTATION

BEIJING | BERLIN | SAN FRANCISCO | SÃO PAULO | WASHINGTON

ACKNOWLEDGMENTS

We thank Heising-Simons Foundation for funding this analysis. Thank you to our colleagues Jennifer Callahan and Dan Rutherford for reviewing earlier versions of this paper.

International Council on Clean Transportation
1500 K Street NW, Suite 650
Washington, DC 20005

communications@theicct.org | www.theicct.org | @TheICCT

EXECUTIVE SUMMARY

Governments and industry are developing plans and policies to reduce climate pollution from all sectors, including international and domestic maritime transportation. Setting a course toward ambitious decarbonization will require confidence that new zero-emission technologies are technically feasible for ships. This study investigates the potential of both liquid and compressed hydrogen fuel cells to replace fossil fuels for bulk carriers, including when paired with wind-assisted propulsion in the form of rotor sails.

We modeled three bulk carriers—a 57,000 deadweight tonne (dwt) coastal dry bulk carrier sailing in China, a 69,000 dwt ore and coal carrier sailing the North American Great Lakes, and a 7,570 dwt cement carrier in northern Europe. We used 2019 Automatic Identification System (AIS) ship traffic data and weather data observations to estimate the ships' total energy use and the energy-saving potential of rotor sails for two routes for each ship. Each route is divided into legs. Ship energy use was estimated with ICCT's Systematic Assessment of Vessel Emissions (SAVE) model. Across the three ships, we found benefits from the rotor sails and a range of port-to-port energy savings of 0.1% to 7.2% per rotor. The two larger ships had lower relative savings compared to the smaller ship because the power generated by the rotor is smaller relative to the total power used by the engines.

Using liquid hydrogen (LH_2), the two larger ships could complete both of their modeled routes even without the help of wind-assisted propulsion. For the Great Lakes bulk carrier— the largest ship—adding rotor sails would reduce fuel consumption and therefore fuel costs by up to 1.4% per rotor. For the Chinese bulk carrier, savings are even larger at up to 3.1% per rotor. As a proportion of total energy use, rotor sails had the greatest energy-saving potential for the European bulk carrier and were capable of port-to-port energy savings up to 7.2% per rotor. With four rotor sails, energy savings of up to 28% or more are possible. However, the smaller European bulk carrier does not have as much space available on board for LH_2, making reliance on hydrogen more challenging for this ship than the other two. Only the shortest of the five legs could be achieved with LH_2 alone. Two other legs could be achieved using rotor sails in combination with LH_2. Its two longest legs could be achieved if it replaced 2.4% of its cargo space with LH_2 in combination with four rotor sails.

Using compressed hydrogen (CH_2), which takes up more space than LH_2 but does not need to be cryogenically stored, presents its own challenges—only the Chinese bulk carrier could use this fuel to complete its typical operations. It could achieve three of the four legs we modeled using CH_2 alone and could achieve the fourth leg with the addition of six rotor sails. The other two ships do not have enough space available to carry enough CH_2 to meet their energy needs along the routes we modeled. A summary of the results of the study are presented in Figure ES-1.

	CH_2	LH_2	Rotor sails
Guangzhou Fa Zahn 1 Length: 200 m DWT: 57,000 t Location: China	3 of 4 legs attained by CH_2 alone 4 of 4 by CH_2 + RS	4 of 4 legs attained by LH_2	Up to 3.1% reduction in fuel use per rotor
Paul R. Tregurtha Length: 309 m DWT: 69,000 t Location: United States	0 of 4 legs attained by CH_2, even with RS	4 of 4 legs attained by LH_2	Up to 1.4% reduction in fuel use per rotor
Ireland Length: 110 m DWT: 7,570 Location: European Union	0 of 5 legs attained by CH_2, even with RS	1 of 5 legs attained by LH_2 3 of 5 by LH_2 + RS 5 of 5 legs by LH_2 + RS + 2.4% CR	Up to 7.2% reduction in fuel use per rotor

CH_2 = compressed hydrogen; LH_2 = liquid hydrogen; RS = rotor sail; CR = cargo space replaced by LH_2

Figure ES-1. Summary of results for the modeled bulk carriers

This research also examined the factors that affect energy savings from rotor sails. We found that energy savings vary depending on wind conditions and are sensitive to wind speed and wind direction. Apparent wind directions across the side of the ship and slightly toward the bow produce the greatest energy savings. Energy savings are also sensitive to how quickly the rotors spin: too slow and they do not generate much thrust; too fast and they consume more energy than they save. The size of the rotor sails also impacts performance, and we found that, all else being equal, taller rotors result in greater energy savings. Lastly, we found that cumulative energy savings increase as the total number of rotors increases.

Ships powered by wind-assisted propulsion paired with liquid hydrogen fuel cells would generate no direct pollution. However, the hydrogen would need to be sourced from renewable energy and not fossil fuels to have climate benefits. Rotor sails reduce the amount of fuel that ships consume and can be retrofitted on existing conventionally fueled ships to reduce fossil fuel consumption; they can also be installed on new ships, including hybrid and zero-emission vessels, to save on energy costs. They can help ships comply with international regulations such as the Energy Efficiency Design Index and Energy Efficiency Existing Ship Index, or domestic regulations that limit the carbon-dioxide-equivalent intensity of ships. Knowing that rotor sails can reduce energy use and emissions for new and existing ships could give governments the confidence to raise the ambition of climate policies.

TABLE OF CONTENTS

LIST OF FIGURES

LIST OF TABLES

INTRODUCTION

For shipping, alternatives to fossil fuels include batteries (Mao et al., 2021), biofuels (Zhou et al., 2020), synthetic electrofuels such as hydrogen (Georgeff et al., 2020; Mao et al., 2020), and wind propulsion (Comer, 2019). To be appropriate for achieving global climate goals, alternatives must generate low or zero carbon-dioxide-equivalent emissions when measured on a life-cycle basis (i.e., well-to-wake).

There are technological, political, social, and economic barriers to replacing fossil fuels with alternative fuels, as detailed by the participants of ICCT's 2019 technical workshop on zero-emission vessel technology (Comer & Rutherford, 2019). For one, alternative fuels are more expensive than fossil fuels. Recent estimates for the price of green hydrogen generated from electrolyzers in the United States and European Union are as low as $0.04/MJ or $0.03/MJ in 2020, respectively (Christensen, 2020); conventional marine fuels, however, sell for around $0.01/MJ.[1] Policymakers and industry might therefore benefit from research that investigates how hydrogen could be paired with wind-assisted propulsion, which can help shipowners comply with climate policies while reducing the costs of using this fuel.

Earlier work showed the potential for liquid hydrogen (LH_2) fuel cells to replace fossil fuels for container ships on the transpacific corridor (Mao et al., 2020). We have also shown the energy-saving and emissions-reduction potential of rotor sails (Comer et al., 2019). Together, these technologies could be used to create zero-emission vessels (ZEVs), and here we investigate whether hydrogen fuel cells could replace fossil fuels for bulk carriers when paired with wind-assisted propulsion in the form of rotor sails.

Whereas hydrogen fuel cells are not yet used on large cargo ships, rotor sails are already in use, and the first order for a newbuild bulk carrier with five tiltable rotor sails was announced in December 2020 (Marshall, 2020). Bulk carriers may be well suited for both hydrogen fuel cells and rotor sails because they potentially have enough space onboard for the fuel cell and hydrogen fuel storage systems, and enough deck space for installing or retrofitting rotor sails. Other wind-assisted propulsion technologies are possible, but here we focus on rotor sails because they are already deployed on several ships, and there is an established and growing market for them.

We investigate three ships using 2019 trade patterns from Automatic Identification System (AIS) data: a 57,000 deadweight tonne (dwt) dry bulk carrier transiting the Chinese coast; a 69,000 dwt ore and coal carrier sailing the North American Great Lakes; and a 7,570 dwt cement carrier operating in Europe's North and Baltic Seas. We chose these ships because they represent a range of sizes that are used in short-sea bulk transportation, and they trade in regions that have pledged to achieve net zero emissions economy-wide by a certain date—the United States by 2050, the European Union by 2050, and China by 2060.

1 Price for H_2 assumes an energy density of 120 MJ/kg; price for conventional fuels assumes very low sulfur fuel oil with an energy content of 42.2 MJ/kg and a fuel price of $500/t.

BACKGROUND

Hydrogen has been used as fuel for over half a century, most notably in space programs as rocket fuel (Granath, 2017). More recently, hydrogen has been used to power cars, buses, trucks, and ferries (Hall et al., 2018). Hydrogen fuel can be used as a compressed gas (CH_2) or a liquid (LH_2), and either used in a fuel cell or an internal combustion engine (ICE). Each of these methods has positives and negatives, and shipping pilot projects are in development or completed for each, as we have summarized in Table 1.

Table 1. Hydrogen-powered vessel projects

Project Name	Vessel type	Hydrogen method	Estimated date of completion	Company	Location	Source
ABB and CFT River Vessel	Cargo transport	LH_2 + fuel cells	2021	ABB, CFT, VTT, and Ballard Power Systems	Europe – France	Flagships (2021)
FreeCO2ast	Pax ferry	LH_2 + fuel cells	2022	Norwegian Electrical Systems, Havyard Design, Havila	Europe – Norway	Osnes (2021)
HydroBingo	Pax ferry	CH_2 + MGO in ICE	2021	CMB and TFC	Japan – Inland Sea	CMB Tech (2021)
Hydrocat	Crew transfer vessel	CH_2 + MGO in ICE	2022	CMB and Windcat Workboats	Europe – Netherlands	CMB Tech (2021)
Hydrogen-fueled demonstration ship	Inland river self-unloading ship	CH_2 + fuel cells	2021	The 605th Research Institute of Chinese State Shipbuilding Corporation	China – Guangdong Province	Fahnestock & Bingham (2021)
Hydrotug	Tugboat	CH_2 + MGO in ICE	2021	ABC and CMB	Europe – Port of Antwerp	CMB Tech (2021)
Hydroville	Passenger shuttle	CH_2 + MGO in ICE	2017	ABC and CMB	Europe – Port of Antwerp	CMB Tech (2021)
HySeas III	Ferry	CH_2 + fuel cells	2021	Ferguson Marine, Government of Scotland	Europe – Scotland	HySeas III Project (2019)
Norled Hydrogen Ferry	Passenger ferry	LH_2 + Fuel cells	2021	Norled, Westcon, Norwegian Public Roads Administration	Europe – Norway	FuelCellsWorks (2020)
NYK Hydrogen-Powered Ferry	Tour boat	H_2 + fuel cells	2024	NYK Line	Japan – Yokohama	Maritime Executive (2020)
NYK Super Eco Ship 2050	Vehicle carrier	LH_2 + fuel cells	Concept study	NYK Line	Japan	NYK Line (2016)
Topeka	Ro-Ro	LH_2 + fuel cells	2024	Wilhelmsen	Europe – Norway	Jiang (2020)
Ulstein SX190 Zero Emission DP2	Offshore support vessel	CH_2 + fuel cells	2022	Ulstein Design & Solutions BV and Nedstack	Europe – Norway	Ulstein (2021)
Water-Go-Round	Passenger ferry	CH_2 + fuel cells	2021	Golden Gate Zero Emission Marine, CARB, SWITCH Maritime	United States – California	Water-Go-Round (2021)
Yanmar EX38A	Fishing vessel	CH_2 + fuel cells	2021	Yanmar and Toyota	Japan – Kunisaki	Butler (2021)
ZeFF	Fast ferry	CH_2 + fuel cells	2020	Selfa Arctic, Norled, Hyon	Europe – Norway	Hyon (2019)

Source: Fahnestock and Bingham (2021)

LIQUID HYDROGEN AND FUEL CELLS

LH_2, or hydrogen that is cooled to cryogenic temperatures until it reaches liquid phase and then stored in insulated tanks, can be used within fuel cells. Minnehan and Pratt (2017) investigated whether hydrogen fuel cells fueled by liquid or compressed

hydrogen are practical in marine applications by considering 14 case studies covering a wide range of vessel types. They studied proton exchange membrane fuel cells and reported advantages of lower operating temperatures and superior gravimetric and volumetric power specifications compared to other types of fuel cells. They developed a method to compare the mass and volume of the required zero-emission solution to the available mass and volume on an existing vessel without changing its current engine and fuel storage systems. They found that hydrogen fuel cells are practically feasible for most of the vessel cases. The fuel cells can be fueled by LH_2 or CH_2. If made using using renewable electricity, the LH_2 or CH_2 can be considered green hydrogen.

In 2020, the ICCT launched a series of zero-emission vessel (ZEV) studies. First, we evaluated the feasibility of replacing fossil fuels with LH_2 fuel cells along a transpacific container shipping route between China and the United States (Mao et al., 2020). That study found that 43% of all voyages could be completed without any modifications to operations or the ships themselves. By adding just one more refueling stop or replacing up to 5% of cargo with LH_2, nearly all of the remaining voyages could be attained using hydrogen. A follow-up study identified where hydrogen refueling stations could be placed along the transpacific corridor to enable a zero-emission trade route between China and the United States (Georgeff et al., 2020).

To give one example, a prototype roll-on/roll-off vessel named the *Topeka* is being developed that will use LH_2 and fuel cells. The vessel is funded by the HySHIP consortium, which is led by a Norwegian shipping operator (Wilhelmsen, 2020). The prototype will run on a 1 MWh battery pack and a specialized 3 MW proton exchange membrane hydrogen fuel cell fueled by filling stations from hydrogen trailers that will supply hydrogen from nearby production plants. It will operate on a fixed route along the coast of Norway and will help establish a LH_2 supply chain.

COMPRESSED HYDROGEN AND FUEL CELLS

Minnehan and Pratt (2017) also considered CH_2 in their study and developed a similar methodology based on comparing the available mass and volume on an existing vessel versus the requirements of fuel cells and pressurized tanks. Their assumptions for a CH_2 system are based on an existing array of 8 tanks of 60 kg capacity. CH_2 can fit into a variety of configurations and tank sizes based on the dimensions of the vessel, but when compared to LH_2, CH_2 will take up more available weight and space given its lower energetic density. With CH_2, there is no extra step to liquefy the fuel and therefore less chance of boil off and energy loss in processing and storage (Global Energy Ventures, 2021; U.S. Department of Energy, 2014).

There are several prototypes of ships using CH_2 and fuel cells. Launching this year is a French river barge on the Seine through a project called Flagships. The vessel, which will be 164 feet in length with 1 MW of power installed, is being built with the goal of carrying exports and imports completely fueled by CH_2 sourced from renewable energy (Flagships, 2021). The project's initial plan was to deploy a push boat in a smaller region, but then it was scaled up to an inland cargo vessel based on potential.

HYDROGEN AND INTERNAL COMBUSTION ENGINES

Hydrogen, either CH_2 or LH_2, can be burned through internal combustion engines (ICE), as is seen in rocket propulsion and hydrogen-fueled cars. In 2017, the Hydroville, the first hydrogen-powered passenger ferry, began operating between Kruibeke and Antwerp during rush hour. It co-combusts CH_2 with diesel fuel in an ICE (Hydroville, 2017). The downside to any fuel being burned through combustion is that it will produce emissions of nitrogen oxides even if the fuel was sourced from renewable energy, and fossil pilot fuel will generate additional air pollution as well as greenhouse

gases. Additionally, ICEs are less efficient than fuel cells, which is why fuel cells are expected to be the preferred option for larger ships (Comer & Rutherford, 2019).

ROTOR SAIL ENERGY-SAVING POTENTIAL FOR SHIPS

In a review of the commercial aeronautic applications of the Magnus effect, Seifert (2012) detailed the early development of rotor sails and their implementation on ships beginning in 1924; a collection of recent studies, described next, has reaffirmed that propulsion can be generated by rotor sails. The thrust generated by rotor sails can offset a portion of a ship's energy use.

Tillig et al. (2018) and Tillig and Ringsberg (2020) developed an operational energy-saving model for ships using rotor sail technology. They tested their ShipCLEAN model for 11 different on-deck rotor sail configurations on two ships, a tanker, and a roll-on/roll-off (ro-ro) vessel. Their model inputs included standard ship dimensions, propeller and engine speed, propeller type, sail dimensions, and the weather conditions along the route. The lift, drag, and power coefficients used in the calculation of power savings within the ShipCLEAN model were based on full-scale observations of rotor sail force balance in real-world sea trials. Assuming an aspect ratio (AR)—the ratio of the rotor height to the rotor diameter—of 6, Tillig and Ringsberg (2020) found maximum cumulative fuel savings of 30% with six rotor sails installed on the tanker and power savings of up to 14% with four rotor sails on the ro-ro ship on a given route. They concluded that the arrangement of the rotors has a large impact on the ship's performance and fuel savings because some rotor sails improved and others declined in performance based on proximity to and interaction with other sails.

De Marco et al. (2016) also considered variables that have been shown to affect system power and efficiency. In their study, simulation of the rotor performance was adjusted to find the performance sensitivity of the spin ratio (SR), which is the ratio of the tangential velocity of the spinning rotor to the apparent wind speed, the AR, and the rotor sail endplates (more on endplates, which are used to improve performance, below). The simulation was then tested with a 205 m long tanker ship and a multirotor setup (AR = 7, height x diameter = 28 m x 4 m). The results suggested that the thrust from simulated rotor sails could offset up to 30% of total power consumption. De Marco et al. (2016) discussed uncertainties in their estimates, including how the tanker simulation did not include hydrodynamic effects, rudder drag, and reduced efficiency of the rotor sail due to ship motions. In a similar computer simulation, Kramer et al. (2016) found ship power reductions of more than 20% using just a single rotor (AR = 5). Kramer et al. (2016) focused on the hydrodynamic effects and how drift and rudder drag affect rotor sail performance.

Talluri et al. (2018) simulated arrangements of rotor sails (AR = 5.1) with two different main engine propulsion systems—gas turbine propulsion and diesel engine propulsion—to evaluate the potential economic and emissions gains. From their analysis of a modeled ro-ro ship with four different route simulations with different weather and ocean conditions, Talluri et al. (2018) found roughly a 20% reduction in total fuel consumption using three rotor sails with diameters of 5 m at once along a simulated route through the Mediterranean Sea for one year. Modeled fuel savings fell to 7% for 3 m diameter rotors with the same AR. Pearson (2014) evaluated the case for retrofitting an existing tanker vessel of 14,700 dwt with two rotor sails (AR = 5), although that study summarized the energy savings by annual performance rather than by route, as in Talluri et al. (2018). For the two rotors, Pearson (2014) found that the annual average reduction in fuel consumption was approximately 10% for a generalized operating profile.

Berendschot (2019) developed a Performance Prediction Program (PPP) model that assesses the fuel consumption of a vessel with rotor sails for any wind condition using a vessel's route and historical weather data. The PPP model predictions compared

favorably to real-world sea trials, and thus an additional case study simulation on the effectiveness of rotor sail retrofit was undertaken to further test various aspects of the PPP. The case study vessel was a 96 m general cargo ship of 4,000 dwt that was outfitted with a single rotor sail (AR = 6, height x diameter = 24 x 4 m) and an 8 m endplate. Berendschot (2019) simulated rotor positions forward and aft on the vessel's weather deck and found the greatest average total fuel savings to be about 13% per voyage with the rotor toward the front of the ship.

From the foregoing review, the overall power savings and reductions in fuel consumption that are possible for regionally sailing vessels utilizing rotor sails appear to be on the order of 5% to 20% per rotor. We attribute the relatively large variation in these estimates to differences in the ships' physical dimensions, inclusion of weather conditions, and underlying assumptions (e.g., spin ratio, aspect ratio, vessel operation speed). Next, we will briefly cover other factors that have been suggested to influence the efficacy of wind-assist technology for maritime applications.

Aerodynamic interactions and sensitivity

Bordogna et al. (2020) investigated the power-saving potential of using dual rotor sail configurations in controlled wind tunnel experiments where the two rotor sails (height = 1.5 m; diameter = 0.3 m; AR = 5) were placed inside a room that was meant to represent the deck of a ship. The relative distances between the two rotor sails were varied to study the impact on resultant aerodynamic forces in a constant wind speed of 5 m s^{-1}. The authors found that increasing the distance between the two rotor sails minimized the aerodynamic interference between them, and greater aerodynamic efficiency occurred when the rotors were placed side by side (one on the port side and one on the starboard side), rather than one behind the other. Tillig and Ringsberg (2020) showed that the optimal rotor sail arrangement also depends on the vessel's hull design, dimensions, and operational speed profile. They further argued that the lift, drag, and power coefficients for the rotor are sensitive to the choice of SR and whether rotor sail endplates are installed. Their experiments showed that the lift, drag, and power coefficients were positively correlated with SR and the size of rotor endplates. Bordogna et al. (2019) suggested that lift, drag, and power coefficients for rotor sails are also sensitive to the air flow's Reynolds number, but their results showed this impact was negligible for an SR greater than 2.5.

Rotor sail endplates

Badalamenti and Prince (2008) focused their study on the effect of installing endplates, or circular caps of varying diameter (D_e) on the upper/lower ends of the rotor sail to determine the optimal design for boosting rotor sail performance. They saw a positive correlation between endplate diameter, documented as a ratio of the rotor sail diameter (D_e/D) and lift coefficient, but concluded that the choice of endplate size will simultaneously influence the drag coefficient, which is also sensitive to SR. They concluded that with endplates, the overall effects on aerodynamic efficiency were modest.

De Marco et al. (2016) simulated operational rotor sail combinations of SR (1–3), AR (2–8), and D_e/D (1–3) and also found that for rotor sails with endplates, the lift coefficient was sensitive to the chosen SR: increasing SR resulted in a larger lift coefficient. If the endplate diameter was assumed constant, the AR also had a positive correlation with the lift coefficient, but lower aerodynamic efficiency was found for the highest D_e/D. In general, D_e/D has an optimal value that can contribute to increasing the efficiency of the rotor sail, but for large D_e/D, the aerodynamic efficiency diminishes.

Aerodynamic and hydrodynamic balance considerations

Previous studies show that several factors contribute to the development of the added resistance forces that impact a vessel with rotor sails installed (Berendschot, 2019;

Kramer et al., 2016; Pearson, 2014; Tillig & Ringsberg, 2019). Side forces from horizontal wind loading on rotor sails protruding above the deck introduce heel and potentially yaw movements depending on where the rotor sail is installed longitudinally along the vessel's center line (Tillig & Ringsberg, 2019). Side forces can also lead to drift angles in the vessel's course, which must be compensated for using the vessel's rudder; wave activity and ensuing vessel motions will also affect rotor sail performance. Thus, changes in aerodynamic factors influence hydrodynamic effects, and some rotor sail performance schemes account for this coupling (Berendschot, 2019). For example, if the side forces induce significant heel and drift beyond what the vessel's rudder is able to counteract, the SR of rotor sails has to decrease, and this reduces the apparent benefits of rotor sails during operation. Therefore, a ship with rotor sails installed will automatically adjust SR using software like the PPP in Berendschot (2019), which monitors the hydrodynamic and aerodynamic conditions in real time to optimize the rotor performance.

METHODOLOGY

Using 2019 ship traffic information for bulk carriers based on AIS data from exactEarth, we searched for routes in three regions: China, North America, and Europe.

For China, bulk carriers are the dominant ship type in its international fleet. The largest bulk cargo terminals in China are in the Bo Sea region, and they transport coal and iron ore both domestically and internationally. The *Guangzhou Fa Zhan 1* is a bulk carrier active in this region, moving coal between the Bo Sea and the Yangtze River Delta. The ship is almost exclusively deployed on this route, which means that if powered by hydrogen, bunkering facilities at the origin and destination ports could be assured of demand.

In North America, bulk carriers on the Great Lakes regularly travel between a handful of major ports. Additionally, Great Lakes bulk carriers are designed to operate only on the lakes and have rounded "bathtub" hulls rather than the v-shaped hulls of oceangoing vessels. Some Great Lakes bulk carriers are so large that they could never leave the lakes because they are too long to pass through the Welland Canal, which bypasses Niagara Falls and separates Lake Erie to the west from Lake Ontario and the St. Lawrence Seaway to the east. The *Paul R. Tregurtha* is the longest ship on the Great Lakes at 309 m, and that also makes it one of the largest bulk carriers in the world.

When searching for bulk carriers operating within the European Union to model, we prioritized smaller carriers to round out our range of vessel sizes. The *Ireland,* smaller than the other two ships, sails near Iceland, which produces geothermal energy covering 25% of the country's overall electricity production and therefore could provide a source of renewable electricity for green hydrogen (Orkustofnun, 2021).

Basic information on each ship is presented in Table 2, and an image of the *Paul R. Tregurtha*, the largest of the three ships, is shown in Figure 1. Note the ample deck space available, which could be used for rotor sails. The *Ireland*, as seen in Figure 2, has existing deck gear installed and may benefit from rotor sails that can be moved on deck to accommodate loading cranes and fixed deck equipment (Anemoi, 2021). Permission to use a photo of the *Guangzhou Fa Zahn 1* was not secured.

Table 2. Characteristics of the bulk carriers modeled in this analysis

Ship name	IMO number	Typical fuel	Installed main engine power (MW)	Deadweight tonnage (t)	Length (m)	Breadth (m)
Guangzhou Fa Zhan 1	9493468	Very low sulfur fuel oil	10	57,000	200	32
Paul R. Tregurtha	7729057	Heavy fuel oil + scrubber	12.5	69,000	309	32
Ireland	9771456	Liquefied natural gas	3	7,570	110	15

Photo credit: The Interlake Steamship Company

Figure 1. The bulk carrier *Paul R Tregurtha* at port.

Photo credit: MF Shipping Group

Figure 2. The cement carrier *Ireland* maneuvering in harbor.

WEATHER DATA

The weather data needed to support the wind-assist modeling aspect of this study includes temperature, eastward wind, northward wind, pressure, and humidity at various altitudes. These variables characterize atmospheric conditions and can also be used to calculate additional variables of interest, such as density and wind direction.

The weather data for this study comes from the ERA5 reanalysis of the European Centre for Medium-Range Weather Forecasts; data was captured at 0.25-degree resolution for all hours of the day during the year 2019 (Hersbach et al., 2020). The ERA5 weather reanalysis is created using a numerical earth system model that incorporates global weather observations from satellites, ground observation stations, buoys, ships/aircraft, instrumented towers, and other equipment to produce hourly estimates of environmental conditions at specific locations. The ERA5 weather data in this report come from an updated version of the environmental data input used by Comer et al. (2019), representing a fourfold increase in spatial resolution and a sixfold increase in temporal resolution from that study. Additional information on the weather data is provided in Appendix A.

ROUTE AND VOYAGE IDENTIFICATION

For each vessel, a dominant route was selected for analysis. On each route, a vessel traverses a certain number of voyages within a given time. Each voyage can comprise one or multiple legs. Figure 3 visually describes the terms *leg*, *voyage*, and *route*.

- *Leg*: Any continuous vessel movement between two full-stop points. *Full-stop* means the vessel shuts down its propulsion engine, and a *point* is usually a terminal at a port.
- *Voyage*: A journey between origin and destination. A voyage may consist of one or more legs.
- *Route*: The pathway between an origin–destination pair. Vessels sail repeated voyages along routes.

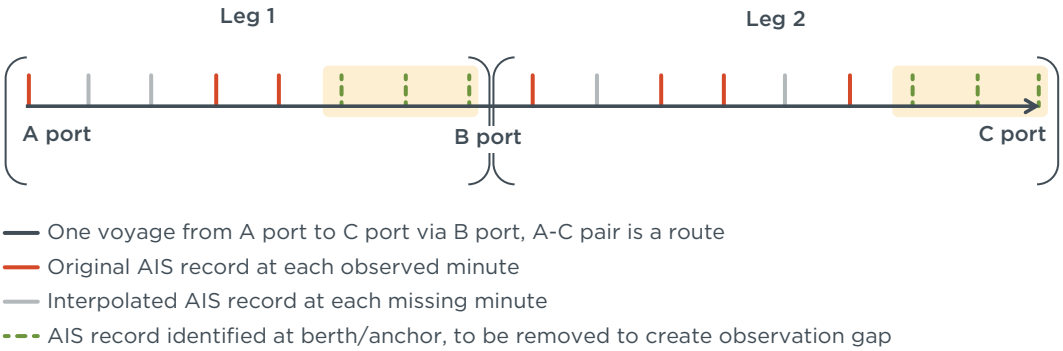

Figure 3. Definition of routes, voyages, and legs, and the identification procedure.

We examined AIS data to identify voyages made by the three selected vessels in 2019. Using ICCT's Systematic Assessment of Vessel Emissions (SAVE) model, we were able to extract hourly ship movement data for the entire year for each sample ship. These data were also identified with one of the four operational phases: cruising, maneuvering into/out of ports, anchoring near ports, and berthing in ports. The information was then fed into a voyage identification algorithm that we adapted from MovingPandas (Graser, 2019), a geospatial analysis tool for extracting trajectories from movement data. AIS data associated with a ship were joined chronologically one point after another until an interruption was detected, such as an observation gap or an anomaly in speed. In our case, these interruptions were times when ships were berthing or anchoring. These gaps split up the whole year of ship activity into multiple segments, each one of which is defined as a leg and assigned a unique identification code (LegID).

Each leg starts and ends at a port, and we combined one or more legs together into routes. Once we have all the legs, we can map them out with traffic flow maps, also enabled by MovingPandas, in order to visualize the routes each ship takes. We then selected the most frequented route plus one additional route for modeling. For each ship, one voyage occurs in colder season and one in the warmer season.[2]

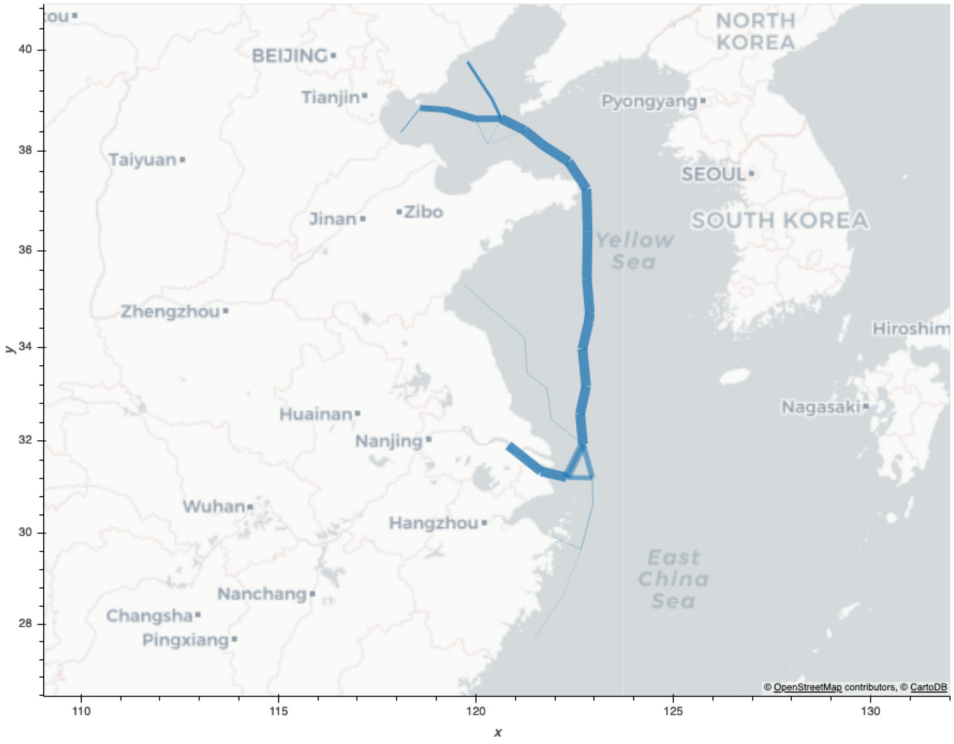

Figure 4. Traffic pattern of the 57,000 deadweight tonne *Guangzhou Fa Zhan 1* in 2019.

Figure 5. Traffic pattern of the 69,000 deadweight tonne *Paul R. Tregurtha* in 2019.

2 We distinguish between cold and warm seasons in relation to the Northern Hemisphere, with October to March being the cold season and April to September being the warm season.

Figure 6. Traffic pattern of the 7,570 deadweight tonne *Ireland* in 2019.

SHIPS AND VOYAGES MODELED

Guangzhou Fa Zhan 1 is a bulk carrier that in 2019 mostly traversed the Bo Sea and Yangtze River Delta region. The route between major iron and coal ports in Bo Sea region (Tangshan Port, Qinhuangdao Port, and Huanghua Port) and dry bulk cargo ports in the Yangtze River Delta region (Nantong Port, Zhangjiagang Port) is around 750 nm and typically takes the ship four days or so to finish. Figure 7 shows the routes we modeled for this ship. Both routes are between Nantong and Tianjin but take slightly different paths.

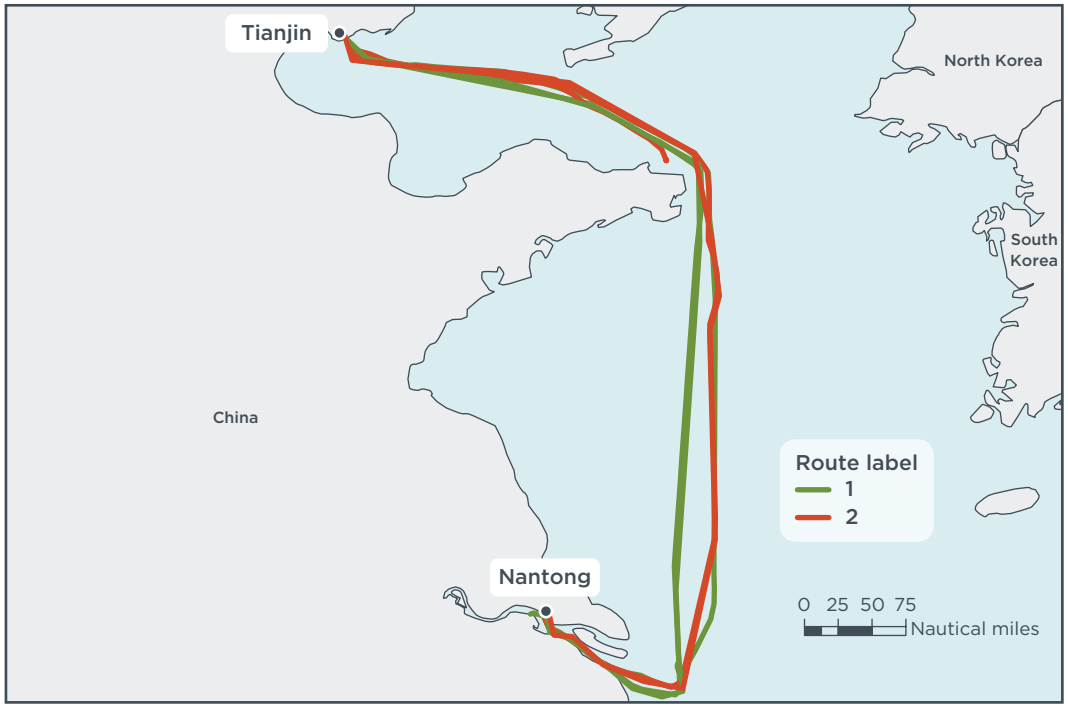

Figure 7. Routes modeled for the 57,000 deadweight tonne *Guangzhou Fa Zhan 1* in 2019.

Paul R. Tregurtha is a bulk carrier transporting iron ore, coal, and stone on the North American Great Lakes. It is the current *Queen of the Lakes*, an unofficial title given to the longest vessel active on the Great Lakes. The most frequent route it traversed in 2019 was between Duluth, Minnesota/Superior, Wisconsin and Monroe, Michigan, which is more than 600 nm one way and takes two to three days to complete. Figure 8 shows the routes we modeled for this ship. Route 3 is between Monroe and Duluth/Superior; route 4 is between Gary and Duluth/Superior and is approximately 740 nm one way.

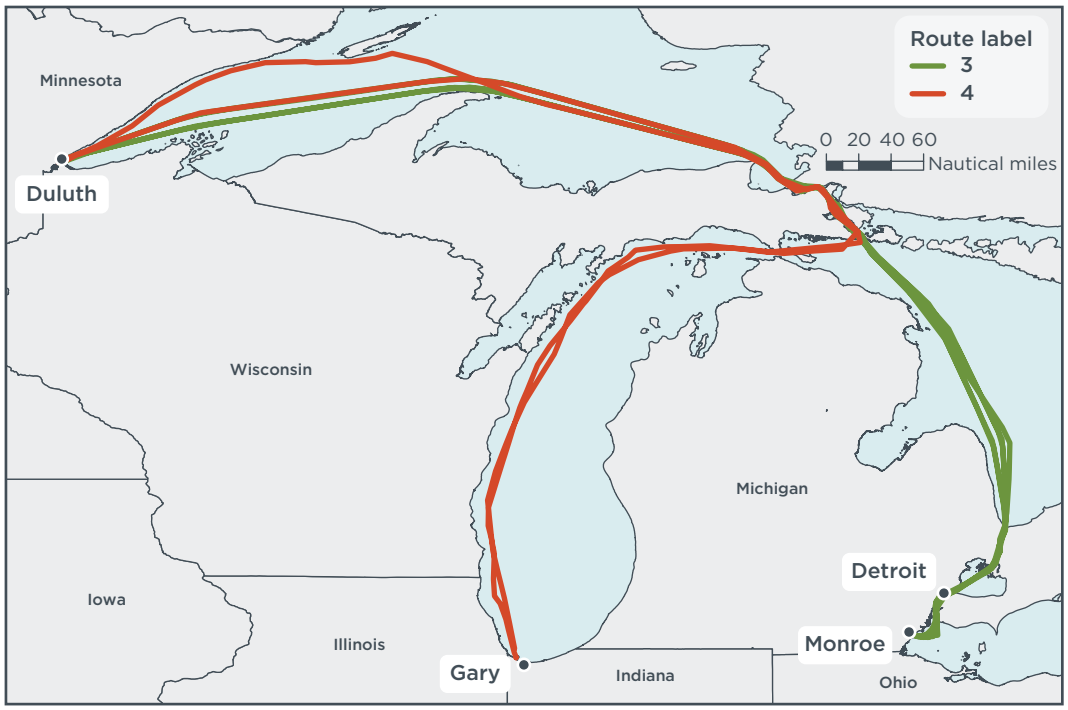

Figure 8. Routes modeled for the 69,000 deadweight tonne *Paul R. Tregurtha* in 2019.

Ireland is a liquefied natural gas–fueled cement carrier. In 2019, the ship was not commissioned to serve a dominant route like the other two, but rather spread out its traffic up and down the coast of Norway in addition to making a handful of prolonged trips to Iceland. Figure 9 shows the routes we modeled for this ship. Route 5 between Brevik and Kjøpsvik consists of 3 legs with distances of approximately 1,140 nm (Brevik to Akranes), 320 nm (Akranes to Akureyri), and 850 nm (Akureyri to Kjøpsvik). Route 6 between Trondheim and Kjøpsvik is approximately 400 nm one way.

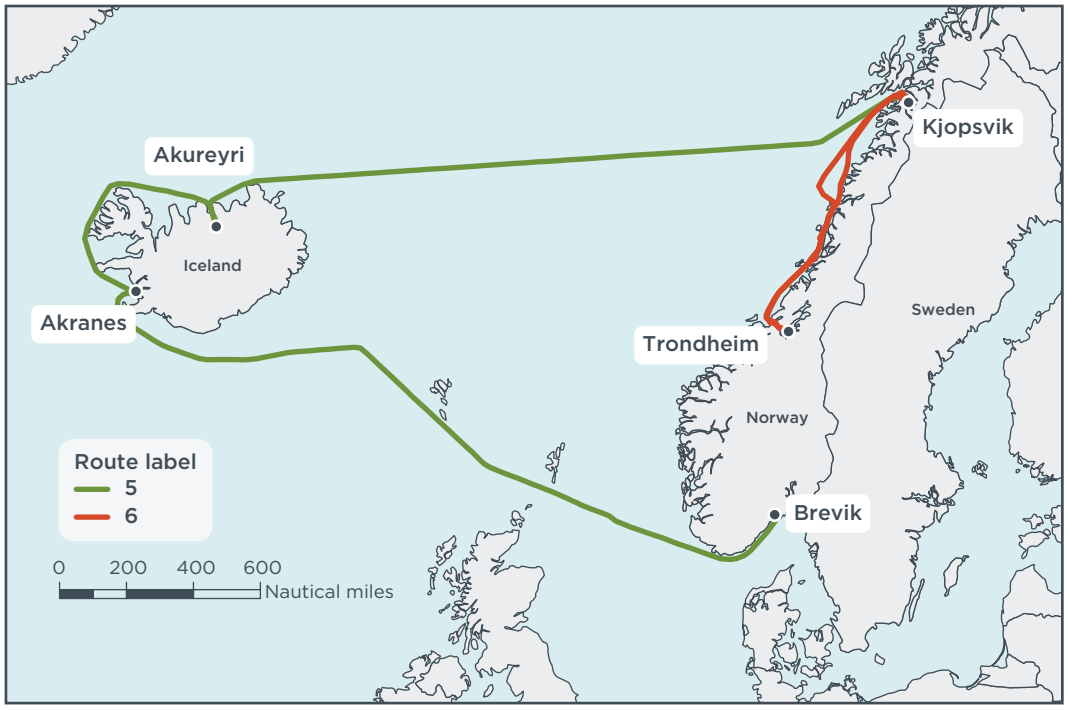

Figure 9. Routes modeled for the 7,570 deadweight tonne *Ireland* in 2019.

ENERGY NEEDS OF THE SHIP

To calculate the energy needs of each ship for voyages along each route, we applied the ICCT's SAVE model (Olmer et al., 2017a, 2017b), which calculates the total energy demand of the ship from the main engines, auxiliary engines, and boilers for each hour. The estimates are based on ship characteristics data from IHS that include installed engine power, maximum speed, and design draught at summer load line as well as AIS ship activity data from exactEarth that include speed over ground and instantaneous draught. SAVE incorporates adjustment factors that account for interpolated speeds, hull fouling, weather, and ballast/loaded conditions, as described in Olmer et al. (2017b). The weather and draught adjustment factors are important for this analysis. The weather adjustment factor is a simple assumption that weather conditions increase main engine power demand on average 10% near shore and 15% away from shore consistent with Smith et al. (2015) and Faber et al. (2020). To operationalize this factor in the SAVE model, Olmer et al. (2017a) defined *near shore* as less than or equal to 5 nm and *away from shore* as greater than 5 nm. The draught adjustment factor (DAF) reduces main engine power demand when the ship is drawing less than its design draught—for example, when the ship is sailing under ballast conditions. The draught adjustment factor is calculated as the ratio of instantaneous draught to design draught raised to the power of 2/3. When the draught ratio is >75%, we assume the voyage is loaded; otherwise we assume it is ballasted.

ENERGY-SAVING POTENTIAL FROM ROTOR SAILS

Rotor sails are vertical spinning columns powered by electric motors on the deck of a ship that generate thrust from the wind through the Magnus effect (Talluri et al., 2018). This wind-generated thrust is the result of balance among aerodynamic forces (i.e., lift and drag) acting on the sails at each moment. At the same time, hydrodynamic forces (i.e., a combination of side, yaw, rudder, and fluid resistance forces) arise in part due to the ocean environment as well as in response to the torques imposed by operating rotor sails (Berendschot, 2019). The amount of propulsion created by an individual rotor sail is often optimized by onboard performance prediction programs assuming coupled aerodynamic and hydrodynamic forces during operation. In this study, we did

not consider the full balance of coupled forces. For the sake of simplicity, we assumed aerodynamic and hydrodynamic forces act on the vessel separately, and we individually considered their impacts on energy savings.

Comer et al. (2019) developed a multistep approach following Lele and Rao (2016), Craft et al. (2012), and De Marco et al. (2016) to estimate fuel savings from rotor sails. For the current paper, we updated the Comer et al. (2019) methodology based on a review of more recent studies by Tillig and Ringsberg (2020) and Bordogna et al. (2019, 2020) and previous work by Badalamenti and Prince (2008), Thouault et al. (2010), and De Marco et al. (2016). Appendix B explains the updates to the methodology.

SPACE REQUIREMENTS FOR HYDROGEN AND FUEL CELLS

We quantified the volume of liquid and compressed hydrogen needed to complete selected voyages and compared it with the amount of hydrogen fuel that could be carried on board. We use the same assumptions and methodologies used in Mao et al. (2020) to estimate the space onboard needed for liquid hydrogen fuel.

Mao et al. (2020) assumed that the density of a liquid hydrogen fuel system is 40 kg/m^3 even though the density of liquid hydrogen is 71 kg/m^3, because the lower figure accounts for the extra space needed for insulated tanks and other fuel system components. This is consistent with Minnehan and Pratt (2017). To estimate the space needed for CH_2 fuel in this study, we applied the same approach as Mao et al. (2020) but adjusted for the lower density of compressed hydrogen. If one accounts for the tank volume needed to store compressed hydrogen at 350 bar, the compressed hydrogen fuel system has a density of approximately 10.7 kg/m^3.[3] This means that nearly four times as much space is needed onboard to hold the same amount of energy in compressed hydrogen form compared to liquid hydrogen.

In some instances, even with liquid hydrogen, the available space on board is not large enough to hold the energy required to complete a leg. In those instances, space reserved for cargo can be replaced with additional fuel. We estimated the amount of cargo space that would need to be converted to fuel storage to complete the leg and compare that to the volume of cargo space available in the same way as Mao et al. (2020).

3 Table 2.3 of Minnehan and Pratt (2017) shows that the liquid hydrogen systems take up 24.8 L/kg, whereas compressed hydrogen systems take up 93.7 L/kg. This is equivalent to 40 kg/m^3 for liquid hydrogen and 10.7 kg/m^3 for compressed hydrogen.

RESULTS

The distance, speed, energy demand, fuel consumption, and other related operational profiles associated with the selected voyages are summarized in Table 3 with the results for both CH_2 and LH_2. Across the three case studies, we found a range of energy savings per rotor of 0.1% to 7.2% per leg, with the lowest energy-saving potentials for the largest ship, the *Paul R. Tregurtha*, and the greatest energy-saving potentials for the smallest ship, the *Ireland*. The *Ireland* also had the largest range in savings, with the highest savings of 7.2% occurring on a leg in August. The *Paul R. Tregurtha* had the smallest range of energy savings, seeing the highest savings in November. The results are affected by wind speed and direction, which vary by season. The impacts of wind speed and direction and seasonality are described in more detail later in this section.

Table 3. Energy savings of rotor sails by voyage, available hydrogen energy by ship, and conditions under which voyages could be attained using a combination of rotor sails and hydrogen.

									Compressed hydrogen		Liquid hydrogen		
Ship	**Date**	**ID**	**Leg**	**Distance (nm)**	**Energy use (MWh)**	**Energy savings per rotor (MWh)**	**Energy savings per rotor**	**H_2 energy available (MWh)**	**Attainable with CH_2 only?**	**Rotors to attain leg with CH_2**	**Attainable with LH_2 only?**	**Rotors to attain leg with LH_2**	**Cargo space replacement and rotor sails needed to attain leg with LH_2**
Guangzhou Fa Zhan 1	Mar 19–21	1A	Nantong → Tangshan	742	329	10.1	3.1%	1,443 LH_2 382 CH_2	**Yes**	0	**Yes**	0	0
Guangzhou Fa Zhan 1	Mar 22–25	1B	Tangshan → Nantong	708	398	3.1	0.8%		No	**6**	**Yes**	0	0
Guangzhou Fa Zhan 1	Aug 28–31	2A	Nantong → Tangshan	720	324	2.3	0.7%		**Yes**	0	**Yes**	0	0
Guangzhou Fa Zhan 1	Sept 1–4	2B	Tangshan → Nantong	722	380	2.4	0.6%		**Yes**	0	**Yes**	0	0
Paul R. Tregurtha	Aug 11–13	3A	Monroe → Duluth/ Superior	611	544	0.8	0.1%	1,679 LH_2 444 CH_2	No	128[a]	**Yes**	0	0
Paul R. Tregurtha	Aug 14–17	3B	Duluth/ Superior → Monroe	638	537	0.4	0.1%		No	264	**Yes**	0	0
Paul R. Tregurtha	Nov 5–7	4A	Gary → Duluth/ Superior	743	657	9.4	1.4%		No	23	**Yes**	0	0
Paul R. Tregurtha	Nov 9–12	4B	Duluth/ Superior → Gary	744	491	5.5	1.1%		No	9	**Yes**	0	0
Ireland	Aug 14–18	5A	Brevik → Akranes	1136	215	15.6	7.2%	76 LH_2 20 CH_2	No	13	No	9	**2.4% + 4 rotor sails (4.5% without rotor sails)**
Ireland	Aug 20–21	5B	Akranes → Akureyri	324	72	0.6	0.9%		No	85	**Yes**	0	0
Ireland	Aug 22–25	5C	Akureyri → Kjøpsvik	852	168	4.6	2.7%		No	33	No	21	**2.4% + 4 rotor sails (3% without rotor sails)**
Ireland	Nov 10–11	6A	Trondheim → Kjøpsvik	398	83	2.1	2.6%		No	30	No	**4**	0
Ireland	Dec 10–11	6B	Kjøpsvik → Trondheim	385	77	3.5	4.6%		No	17	No	**1**	0

[a] Red font indicates unreasonable number of rotor sails would be required to attain the leg with hydrogen.

Only the *Guangzhou Fa Zahn 1* was able to complete three out of four voyages using CH_2. Neither the largest ship, the *Paul R. Tregurtha*, nor the smallest ship, the *Ireland*, had the capacity on board to hold enough fuel to attain any of their legs with CH_2 alone or in combination with rotor sails. Meanwhile, both the *Guangzhou Fa Zahn 1* and the *Paul R. Tregurtha* could carry more than enough LH_2 on board to complete voyages along their regular routes using LH_2 fuel cells. The *Guangzhou Fa Zahn 1* can store nearly 1,500 MWh of LH_2 energy on board, whereas a typical leg requires between 300 and 400 MWh to complete. Similarly, the *Paul R. Tregurtha* can store about 1,700 MWh of LH_2 energy on board, and its legs require between approximately 500 and 650 MWh to complete. Even though these ships do not need rotor sails to complete these legs, we found that they would benefit from the energy savings thus generated. Adding rotor sails would reduce hydrogen fuel consumption by up to 3.1% per rotor for the *Guangzhou Fa Zahn 1* and up to 1.4% for the *Paul R. Tregurtha*. The *Guangzhou Fa Zahn 1* could complete its unattained voyage by installing 6 rotor sails on board. The impacts of each technology combination are described in Figure 10.

	CH_2	LH_2	Rotor sails
Guangzhou Fa Zahn 1 Length: 200 m DWT: 57,000 t Location: China	3 of 4 legs attained by CH_2 alone 4 of 4 by CH_2 + RS	4 of 4 legs attained by LH_2	Up to 3.1% reduction in fuel use per rotor
Paul R. Tregurtha Length: 309 m DWT: 69,000 t Location: United States	0 of 4 legs attained by CH_2, even with RS	4 of 4 legs attained by LH_2	Up to 1.4% reduction in fuel use per rotor
Ireland Length: 110 m DWT: 7,570 Location: European Union	0 of 5 legs attained by CH_2, even with RS	1 of 5 legs attained by LH_2 3 of 5 by LH_2 + RS 5 of 5 legs by LH_2 + RS + 2.4% CR	Up to 7.2% reduction in fuel use per rotor

CH_2 = compressed hydrogen; LH_2 = liquid hydrogen; RS = rotor sail; CR = cargo space replaced by LH_2

Figure 10. Summary of results for the modeled bulk carriers.

The *Ireland* does not have as much space available and can carry 76 MWh of LH_2 or 20 MWh of CH_2 energy onboard. Its legs require between 72 and 215 MWh to achieve, and therefore it could complete only the shortest leg of one of its voyages, 324 nm, with a LH_2 powered fuel cell with no further modifications. Detailed results for LH_2 for this ship by leg are illustrated in Figure 11. We are highlighting this ship to demonstrate how rotor sails can make the difference in achieving legs with hydrogen alone or in combination with cargo replacement. The other two ships do not need rotor sails to run on hydrogen but benefit from them through fuel savings. Adding one rotor sail results in achieving the second shortest leg (6B; 385 nm), and adding four rotor sails would result in achieving the third shortest (6A; 398 nm).

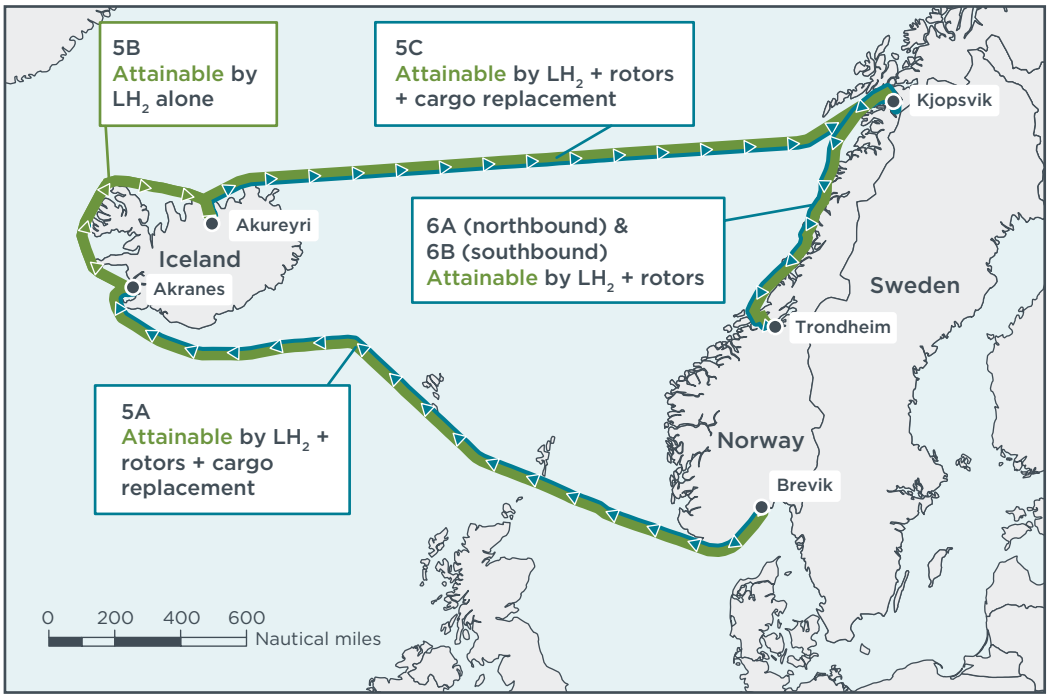

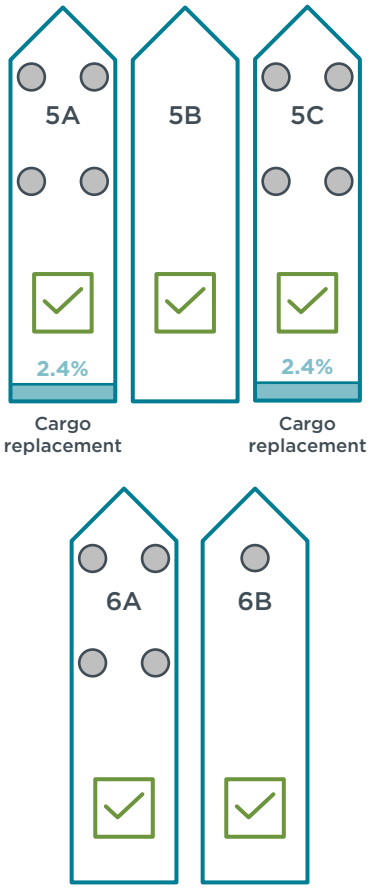

Note: Ship diagram not to scale and rotor sail placement is for illustration purposes only.

Figure 11. Summary of the results for the 7,570 dwt bulk carrier using LH_2 fuel cells and rotor sails.

The *Ireland's* two other legs that could not be achieved with LH_2 would require either 9 or 21 rotor sails to complete, and these are unreasonable numbers. No ship has installed more than five rotor sails to date (Marshall, 2020). For the *Guangzhou Fa Zahn 1*, six rotor sails are theoretically possible, as seen in the configurations by Tilling and Ringsberg (2020). But still, adding additional rotor sails increases the chances of interactions between rotors, which leads to decreased efficiency, increased conflict with normal operations (e.g., loading/unloading, access to cargo holds), decreased visibility, and increased stability concerns (Talluri et al., 2018).

We estimated per-rotor energy savings of 0.9% to 7.2% for the *Ireland*. With four rotor sails, energy savings of up to 28% or more are theoretically possible. For the *Ireland's* two legs that were not achievable by adding rotor sails, we estimated how much cargo space would need to be allocated to additional fuel to achieve the remaining legs. If we assume that cement takes up 0.69 m^3/t, then the interior volume of the cargo space is approximately 5,250 m^3 for the 7,570 dwt *Ireland*.[4] Therefore, by replacing 2.4% of cargo space and utilizing four rotor sails, legs 5A and 5C could be attained. Without the rotor sails, the *Ireland* would need to replace 4.5% of cargo space with fuel to attain 5A and 3% to attain 5C. Therefore, rotor sails can not only reduce fuel consumption but also enable ships to avoid replacing cargo with fuel. Note that the orientation of the rotor sails in Figure 11 might not be optimal, and other arrangements are possible.

EFFECT OF WIND SPEED AND DIRECTION

We found that energy savings from rotor sails vary depending on wind conditions. The average apparent wind conditions for each domain/vessel are shown in Figure 12.

4 Assumes cement has a density of 1.44 t/m^3, which is 0.69 m^3/t, and 7,570 dwt * 0.69 m^3/t = 5,256 m^3.

In this case, the apparent winds were binned and subsequently averaged by azimuth. Our data suggest that the strongest apparent wind is found in the season that would have the strongest background wind conditions (i.e., true wind), and in the Northern Hemisphere those typically occur throughout the winter months from October through March. We also note generally weaker average apparent wind speed during the summer months, April through September. The background true wind could be favorable in terms of speed, but maximizing the potential energy savings at each hour requires that the vessel travel on a favorable course for optimizing the relative inflow.

The relative inflow—in other words, the apparent wind velocity—is therefore important to consider along each leg. For legs 1B and 2A (top panel in Figure 12), the apparent wind speed is greater than 10 m s^{-1}, but the apparent wind angle is unfavorable for generating appreciable energy using rotor sails (<45°). Moreover, the *Guangzhou Fa Zhan 1* experienced poor apparent wind conditions for more than 60% of the duration of leg 2A. Meanwhile, the apparent wind conditions were favorable across much of leg 1A. For the *Paul R. Tregurtha* in North America (middle panel), the apparent wind speeds were generally less than 7 to 8 m s^{-1} for each leg except for 4A (a winter leg). However, the apparent wind angle was unfavorable for generating large energy savings via the use of rotor sails because headwinds were encountered for about 50% of the leg. Finally, in Europe, the *Ireland* (bottom panel) experienced headwinds for the majority of each leg. We note that the largest energy-saving potential is found for moderate apparent wind speeds of about 7 to 8 m s^{-1}, at favorable apparent wind angles of about 90° to 150°, which occurred for roughly 30% to 40% of the duration of leg 5A.

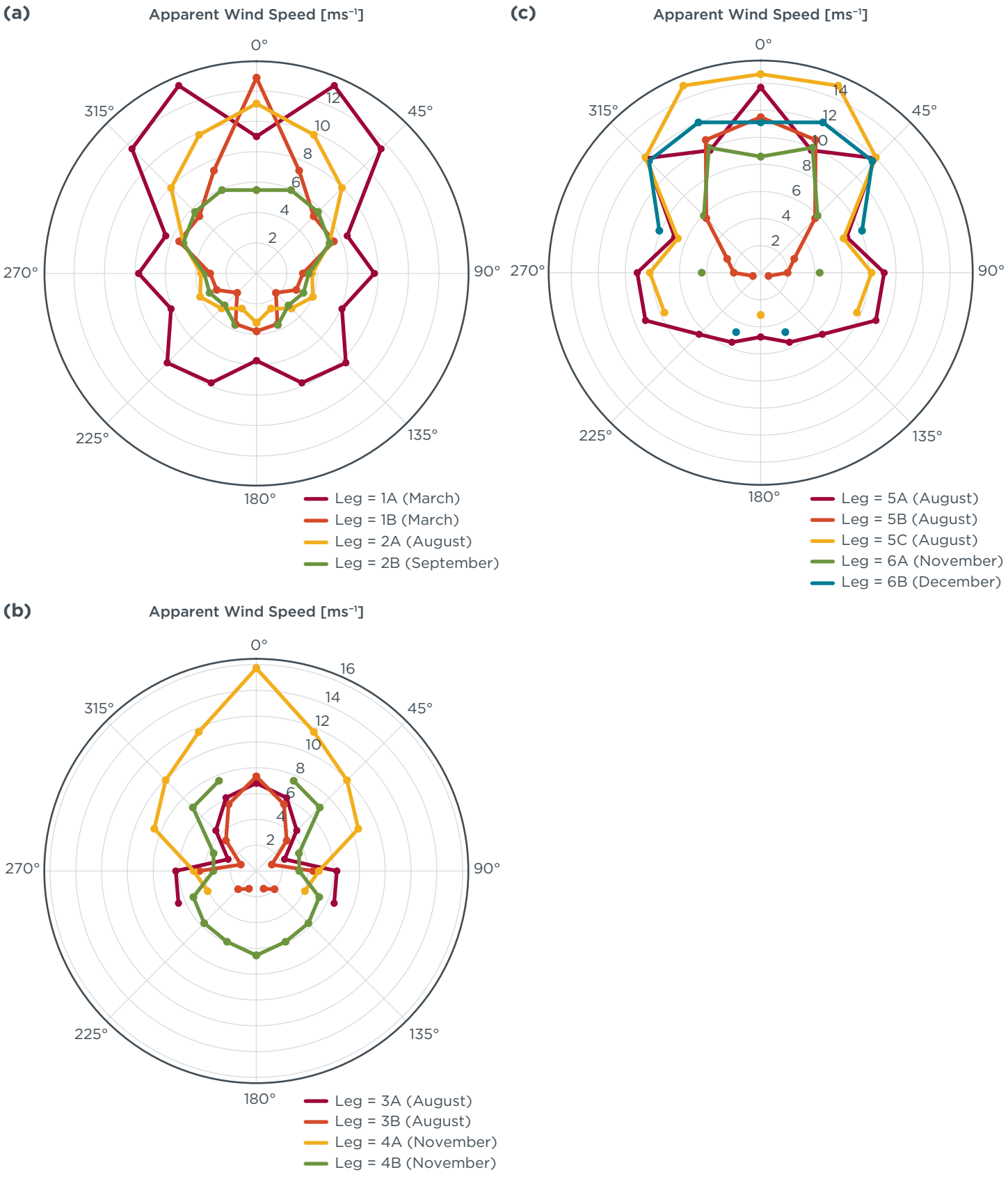

Figure 12. The average apparent wind speed for all legs in the Asian (a), North American (b), and European (c) routes as a function of apparent wind direction.

Figure 13 further illustrates that the net energy savings generated using rotor sails is sensitive to the apparent wind speed and apparent wind direction together. Below

apparent wind speeds of about 5 to 7 m s^{-1}, energy savings from rotor sails are minimal (generally <50 kWh), regardless of the apparent wind direction. However, once the apparent wind speed exceeds this rough wind speed threshold, the maximum net energy savings are found between apparent wind angles of approximately 40° to 140°. Following the aerodynamic theory of rotor operation from Tillig & Ringsberg (2020) and references therein, and assuming a SR of 3.0, the maximum forward thrust is predicted for an apparent wind angle of ~+/- 100° to 110° relative to the ship's bow.

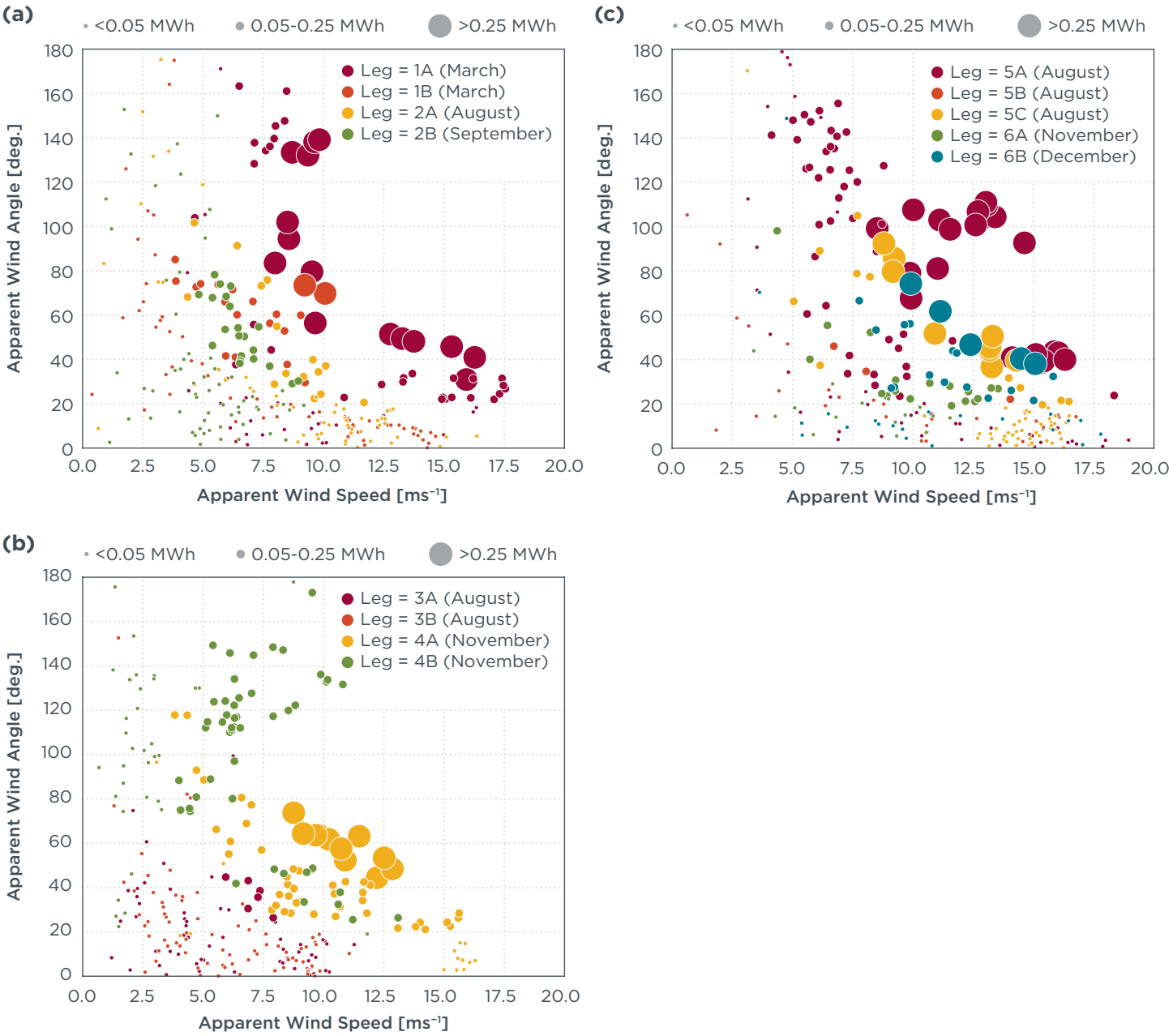

Figure 13. Net energy savings generated using rotor sails as a function of apparent wind angle and apparent wind speed for routes in Asia (a), North America (b), and Europe (c).

SEASONALITY

Figure 14 shows that the cumulative net energy savings generated using a single rotor are maximized by conducting voyages during the windier season(s). For example, the cumulative net energy savings generated by 50 hours from origin in the Great Lakes domain for the winter (November) voyages is about three to four times greater compared to the voyages in the summer (August) season. This finding is generally

consistent across all the domains studied. The energy savings calculated out to 40 hours from origin for the ship in China are larger for legs in March and in Europe for legs in November and December. Although legs 5A (red solid) and 5C (yellow) in August 2019 in Europe generate significant cumulative energy savings, this is likely due to the accumulation of minor gains over relatively long journeys. In addition, some seasonal differences in the energy-saving potential may result from vessels traveling within inshore reaches of the domain, where the overall wind speed tends to be lower on average (Ahsbahs et al., 2017).

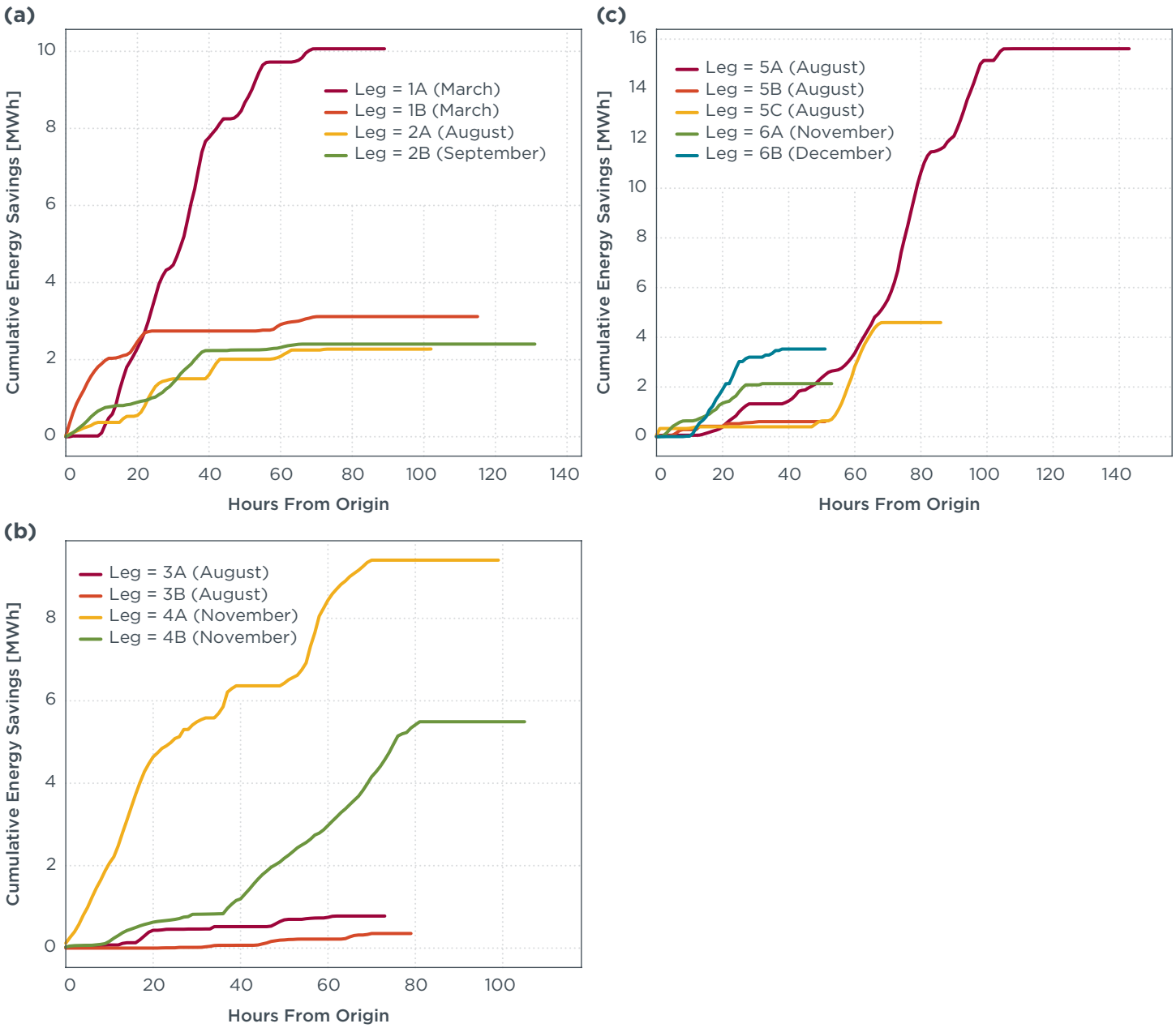

Figure 14. The cumulative net energy savings (generated using rotor sails for each leg of each voyage in Asia (a), North America (b), and Europe (c).

ROTOR SAIL SENSITIVITY ANALYSIS

Our results are sensitive to SR and rotor size. The above results are for an SR of 3, which implies that the rotor sails are throttled up or down so that the rate of rotation of the rotor sail is a factor of three times the apparent wind speed. In practice, though, the rotor sails can be operated within some range within their original engineering design specification. Therefore, SR can vary.

As shown in Figure 15, the net energy generation potential is highly sensitive to the choice of SR during operations. From these simulations, an SR of 3 or 4 appears to generate the maximum energy-saving potential using rotor sails. When the SR is small—for example, 1—the net thrust is small. When the SR is large—for example, 6—the energy required to spin the rotor increases faster than the net thrust increases, resulting in lower net energy generation potential compared to an SR of say 5. Varying the SR will also change the relative balance of lift, drag, and power consumption, and there will be resultant changes in the apparent wind angle for which maximum thrust is achieved for a given true wind condition.

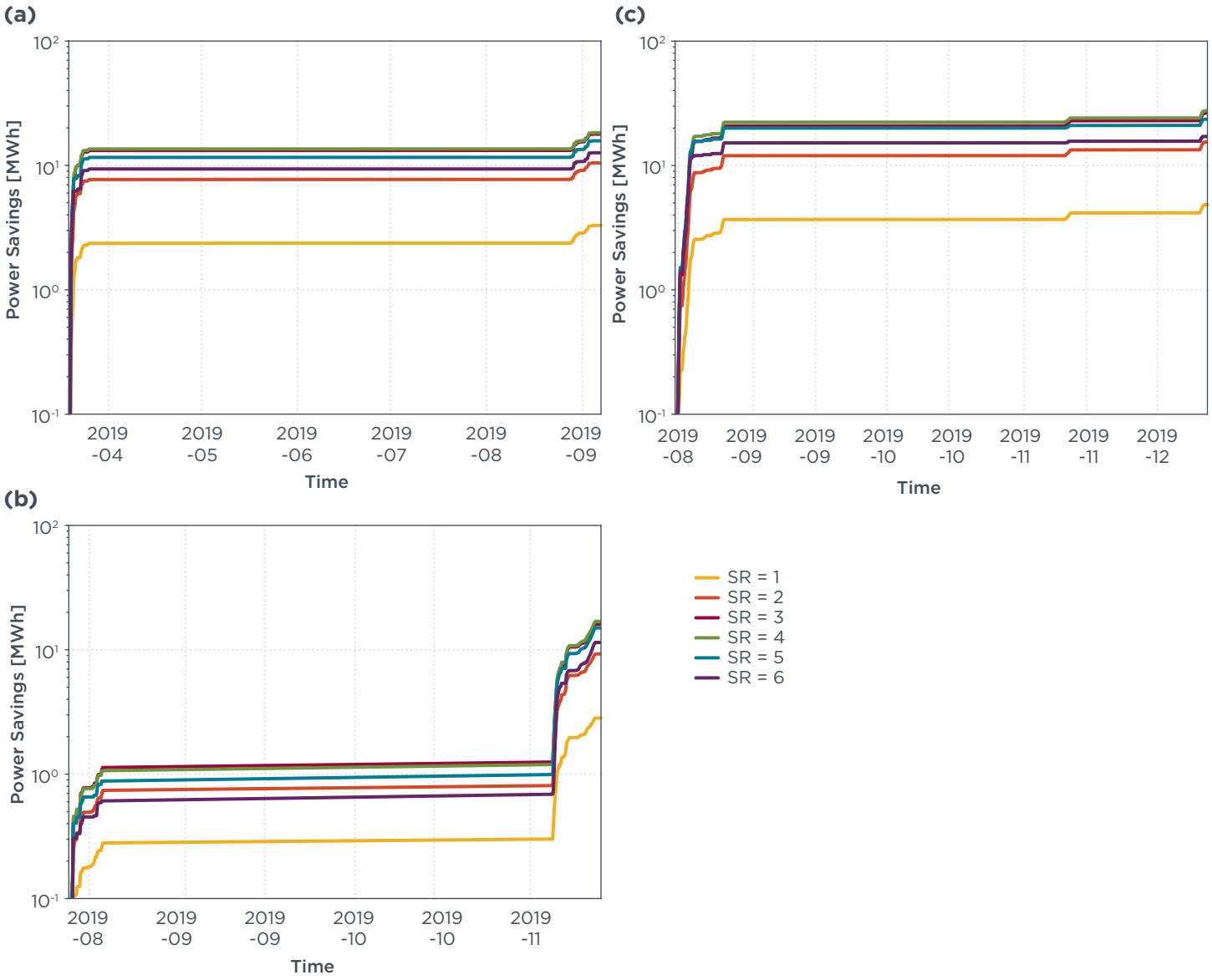

Figure 15. The cumulative net energy generated by rotor sails as a function of spin ratio for example legs in Asia (a), North America (b), and Europe (c).

As shown in Figure 16, the energy-saving potential of rotor sails will vary according to the dimensions of the rotor. If we assume a constant AR of 6 and vary the height and diameter of the rotor, we observe proportional changes in energy-saving potential. For the variations in rotor dimensions considered in this simple experiment, we demonstrate considerable sensitivity to rotor size: as much as 40% to 50% in terms of relative energy generation potential depending on the dimension of the chosen rotor sails.

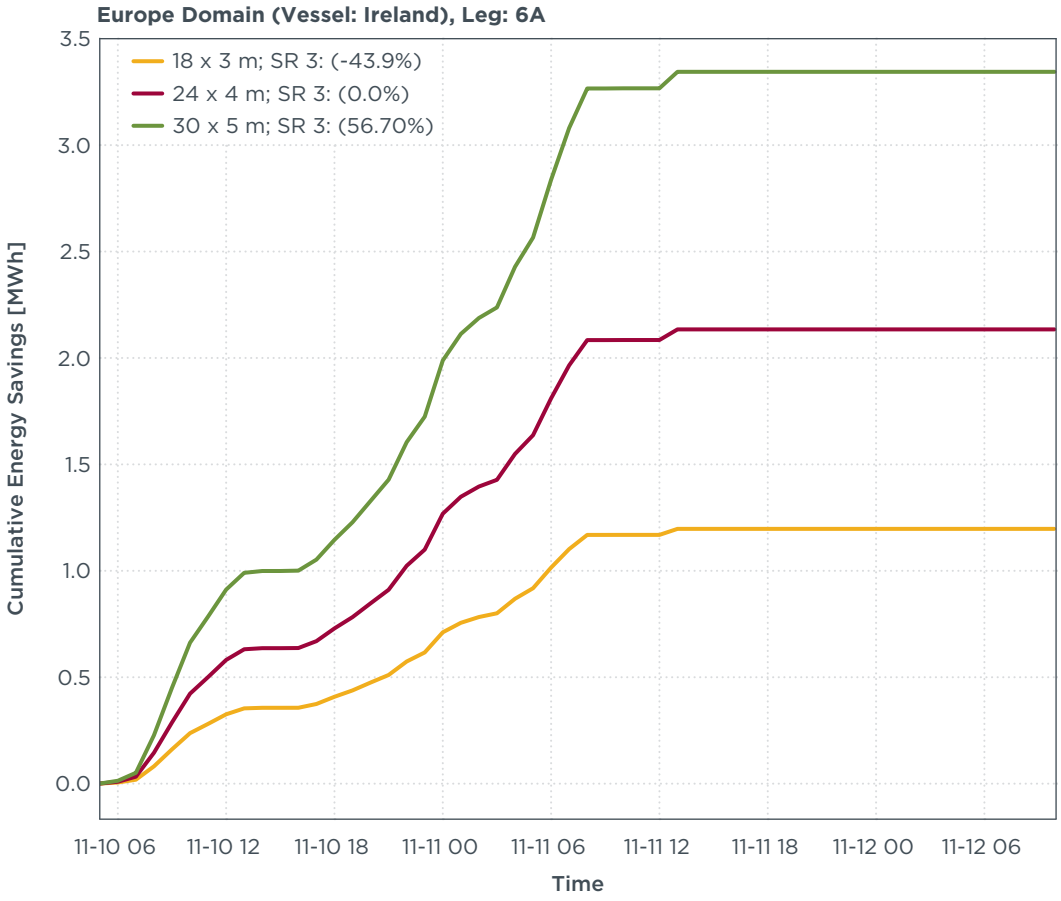

Figure 16. Cumulative net energy generated using rotor sails as a function of height and diameter while maintaining an aspect ratio of 6 for an example leg.

COMPARISON WITH OTHER STUDIES

For the hydrogen fuel cell capabilities, our results coincide with previous findings from Mao et al. (2020), because the LH_2 fuel cells enabled our two larger ships—which would be classed as medium size in the Pacific-wide Mao et al. study—to complete all legs, given the greater available space for the fuel cells. Our two larger ships also had no need to add rotor sails to complete any of their legs. Like Mao et al. (2020), we found that replacing cargo space with fuel enables ships to attain their voyages using hydrogen fuel when they would not be able to otherwise. We found that using rotor sails can cut the amount of cargo space that needs to be replaced with hydrogen fuel in half in some cases. Like Minnehan and Pratt (2017), we found that using LH_2 enables ships to complete more voyages than CH_2 because more energy is contained per unit volume in LH_2 than CH_2.

Regarding the energy-saving potential of rotor sails, our findings are most directly comparable with Berendschot (2019), which, like our study, modeled the impacts of individual rotors with an AR of 6 (height x diameter = 24 x 4 m) combined with historical wind data along an actual route from Rotterdam to Casablanca. Berendschot (2019) estimated that one rotor sail mounted on the front of the ship reduced fuel consumption by approximately 13% round trip. We found route-level fuel savings of up to 7.2% per rotor. Berendschot's (2019) per-rotor savings may be higher because the model used in that study optimizes the performance of the rotor along the modeled route. This comparison suggests our findings may be conservative.

Other studies assessing savings from rotor sails, including Tillig and Ringsberg (2020), Bordogna et al. (2019), De Marco et al. (2016), and Talluri et al. (2018), are not directly comparable to ours because the vessels in those studies had more than one rotor sail (up to 6) or multiple rotor configurations on the deck of the ship, or because the research was done in a laboratory setting. Still, these studies found between 20% and 36% voyage-level savings while using the rotor sails, and if one were to simply divide the amount of savings by the number of rotors, energy savings are toward the higher end of our findings. For example, Tillig and Ringsberg (2020) found between 5% and 7% fuel savings per rotor, and Talluri et al. (2018) found approximately 6% fuel savings from a single rotor. These studies collectively put forth a relatively strong argument for installation of multiple rotors aboard a ship for maximum fuel savings. However, there must often be a balance between savings and the expense of installations for multiple rotors, as a single 5 m diameter rotor can cost half a million U.S. dollars (Talluri et al., 2018).

Aside from the savings provided, other operational characteristics of the rotor sails were confirmed. We found that apparent wind direction is more pertinent to maximizing power savings than wind speed along a given route. This finding is similar to that of Talluri et al. (2018), which also found that apparent wind direction had a greater impact on performance of the rotor sail than apparent wind speed. Additionally, we found that the cumulative energy savings are sensitive to the choice of SR, and an SR of 3 or 4 appears to generate the maximum power-saving potential. De Marco et al. (2016) considered SRs up to 3 and found that the higher the SR, the higher the lift coefficients. Although De Marco et al. (2016) noted that SR values for marine propulsion are currently between 1 and 3, the maximum possible angular velocity attainable by rotor sails has been increasing over the years, allowing for higher SRs.

Other studies have also found an influence of rotor size on performance. Although we maintained an AR of 6 and used the dimensions of 24 m x 4 min in our results, we did a sensitivity analysis investigating other dimensions that still had an AR of 6, namely 18 m x 3 m and 30 m by 5 m. We found that the larger the dimensions, the higher the power savings, as a direct result of the increase in projected area exposed to the apparent wind. This finding is consistent with Talluri et al. (2018).

Future work could address the potential for aerodynamic interactions between multiple rotor sails operating together by utilizing simplified power reduction approaches—for example, using the methods of Bordogna et al. (2019) and references therein. It could also incorporate more specific hydrodynamic resistance assumptions based on vessel dimensions and wave data. Studies could focus on identifying optimal routes based on concurrent weather and ocean conditions, rightsizing the rotor sails for the ship and its operating conditions, and allowing rotor parameters like SR to vary to optimize their performance. Lastly, future work could model the performance of wind-assisted propulsion across a larger number of ships over the course of an entire year or several years; this would help researchers better understand the potential benefits of wind-assisted propulsion as shipowners consider ways to reduce fuel costs and comply with environmental and climate regulations.

CONCLUSIONS

We estimated ship energy use and potential energy savings from wind-assisted propulsion in the form of rotor sails to determine whether liquid or compressed hydrogen fuel cells could replace fossil fuels for bulk carriers when paired with rotor sails. Three bulk carriers were modeled: a 57,000 dwt coastal dry bulk carrier sailing in China, a 69,000 dwt ore and coal carrier sailing in the Great Lakes, and a 7,570 dwt cement carrier in Europe. We used actual ship traffic data from AIS paired with weather model data to estimate the energy use and the energy-saving potential of rotor sails for two voyages for each ship.

For the rotor sails, results show a range of port-to-port energy savings of 0.1% to 7.2% per rotor. Larger ships had lower relative savings compared to smaller ships because the power generated by the rotor is smaller relative to the power used by the engines. As a proportion of total energy use, rotor sails had the greatest energy-saving potential for the European bulk carrier and were capable of port-to-port energy savings up to 7.2% per rotor. With four rotor sails, energy savings of up to 28% or more are theoretically possible. In general, we predict lower energy savings than the literature, suggesting our results may be conservative. The reasons may be because others modeled hydrodynamic forces in a detailed way, whereas we used simple multipliers to account for extra power requirements for the ship to overcome wind and waves. Additionally, unlike some other researchers, we did not vary any parameters such as spin ratio to optimize the performance of the rotor sails.

When hydrogen-powered ships enter the market, it will be important for routes to be matched to the right ship. For example, smaller ships like the European bulk carrier we modeled can achieve zero-emission voyages using fuel cells on shorter distance voyages, whereas larger ships with larger volume capacities to hold fuel cells and hydrogen can achieve longer zero-emission voyages. In all cases, wind-assist technology can be used to both increase fuel savings and extend the range of all ships, including those powered by hydrogen fuel cells. This was the case for the Chinese bulk carrier and for some of the legs of the European bulk carrier, which were able to attain previously unattained voyages using fuel cells with the addition of rotor sails. While wind-assisted propulsion helped the European bulk carrier achieve some unattained legs, several remained unattained, meaning that a portion of the ship's cargo space would need to be replaced with additional hydrogen fuel. Even in these instances, wind-assisted propulsion provided a benefit. We found that using four rotor sails would cut the amount of cargo space that needed to be replaced with hydrogen fuel from 3% or 4.5% to just 2.4%.

This research also produced some insights into the factors that affect energy savings from rotor sails. We found that energy savings vary depending on wind conditions and are sensitive to wind speed and wind direction. Winter voyages tended to have higher energy-saving potentials than other times of year due to higher wind speeds. Apparent wind directions across the side of the ship and slightly toward the bow produce the greatest energy savings. Energy savings are also sensitive to the spin ratio, with optimal savings at spin ratios of between 3 and 4. The size of the rotor sails also impacts performance. All else equal, taller rotors result in greater energy savings. Lastly, we find that cumulative energy savings increase as the total number of rotors increases. Future work could improve how hydrodynamic factors are accounted for, allow for optimized rotor performance, and model energy savings over the course of an entire year or several years rather than discrete voyages and routes.

This study shows that wind-assisted propulsion can be paired with liquid hydrogen fuel cells, which would result in ships that generate no direct pollution. However, the hydrogen would need to be sourced from renewable energy and not fossil fuels to have climate benefits. Rotor sails reduce the amount of fuel that ships consume and can be

retrofitted on existing conventionally fueled ships to reduce fossil fuel consumption; they can also be installed on new ships, including hybrid and zero-emission vessels, to save on energy costs. They can help ships comply with international regulations such as the Energy Efficiency Design Index and Energy Efficiency Existing Ship Index, or domestic regulations that limit the carbon-dioxide-equivalent intensity of ships. Knowing that rotor sails can reduce energy use and emissions for new and existing ships could give governments the confidence to raise the ambition of climate policies.

REFERENCES

Anemoi. (2021). Rotor Sail Technology—Anemoi Marine. London, England: Anemoi Marine Technologies Ltd. Retrieved from https://www.anemoimarine.com/rotor-sail-technology/

Ahsbahs, T., Badger, M., Karagali, I., & Larsén, X. G. (2017). Validation of Sentinel-1A SAR coastal wind speeds against scanning LiDAR. *Remote Sensing*, *9*(6), 552. https://doi.org/10.3390/rs9060552

Badalamenti, C., & Prince, S. (2008, August 18). *The effects of endplates on a rotating cylinder in crossflow*. Presented at the 26th AIAA Applied Aerodynamics Conference, Honolulu, Hawaii. https://doi.org/10.2514/6.2008-7063

Berendschot, R. J. (2019). *Flettner rotor vessel design optimisation.* [Master thesis]. Delft, Netherlands: Delft University of Technology. Retrieved from https://repository.tudelft.nl/islandora/object/uuid%3A83f8c10d-2407-4107-b545-3ab9bd3b0991

Bordogna, G., Muggiasca, S., Giappino, S., Belloli, M., Keuning, J. A., & Huijsmans, R. H. M. (2020). The effects of the aerodynamic interaction on the performance of two Flettner rotors. *Journal of Wind Engineering and Industrial Aerodynamics*, *196*, 104024. https://doi.org/10.1016/j.jweia.2019.104024

Bordogna, G., Muggiasca, S., Giappino, S., Belloli, M., Keuning, J. A., Huijsmans, R. H. M., & van 't Veer, A. P. (2019). Experiments on a Flettner rotor at critical and supercritical Reynolds numbers. *Journal of Wind Engineering and Industrial Aerodynamics*, *188*, 19–29. https://doi.org/10.1016/j.jweia.2019.02.006

Butler, J. (2021, April 5). 1st sea trial of Yanmar/Toyota hydrogen fuel cell boat. Toronto, Canada: Plugboats. Retrieved from https://plugboats.com/1st-sea-trial-yanmar-toyota-hydrogen-fuel-cell-boat/

Christensen, A. (2020). *Assessment of hydrogen production costs from electrolysis: United States and Europe*. Washington, DC: International Council on Clean Transportation. Retrieved from https://theicct.org/publications/assessment-hydrogen-production-costs-electrolysis-united-states-and-europe

CMB.TECH. (2021). Marine Projects. Antwerp, Belgium: CMB.TECH. Retrieved from https://cmb.tech/solutions/marine

Comer, B., Chen, C., Stolz, D., & Rutherford, D. (2019). *Rotors and bubbles: Route-based assessment of innovative technologies to reduce ship fuel consumption and emissions*. Washington, DC: International Council on Clean Transportation. Retrieved from https://theicct.org/publications/working-paper-imo-rotorships

Comer, B., & Rutherford, D. (2019, July 9). *Workshop summary: ICCT technical workshop on zero emission vessel technology*. Washington, DC: International Council on Clean Transportation. Retrieved from https://theicct.org/sites/default/files/ZEV%20workshop%20summary_vf.pdf

Craft, T. J., Iacovides, H., Johnson, N., & Launder, B. E. (2012). *Back to the future: Flettner-Thom rotors for maritime propulsion?* THMT-12. Proceedings of the Seventh International Symposium on Turbulence, Heat, and Mass Transfer, Palermo, Italy, 24–27 September 2012. https://doi.org/10.1615/ICHMT.2012.ProcSevIntSympTurbHeatTransfPal.1150

Da-Qing, L., Leer-Anderson, M., & Allenstrom, B. (2012). *Performance and vortex formation of Flettner rotors at high Reynolds numbers.* Proceedings of 29th Symposium on Naval Hydrodynamics, Gothenburg, Sweden, August 26–31.

De Marco, A., Mancini, S., Pensa, C., Calise, G., & De Luca, F. (2016). Flettner rotor concept for marine applications: A systematic study. *International Journal of Rotating Machinery*, *2016*, 1–12. https://doi.org/10.1155/2016/3458750

Faber, J., Hanayama, S., Zhang, S., Pereda, P., Comer, B., Hauerhof, E., Schim van der Loeff, W., Smith, T., Zhang, Y., Kosaka, H., Adachi, M., Bonello, J.-M., Galbraith, C., Gong, Z., Hirata, K., Hummels, D., Kleijn, A., Lee, D., Liu, Y., … Yuan, H. (2020). *Fourth IMO greenhouse gas study*. London, England: International Maritime Organization. Retrieved from https://www.imo.org/en/OurWork/Environment/Pages/Fourth-IMO-Greenhouse-Gas-Study-2020.aspx

Fahnestock, J., & Bingham, C. (2021). *Mapping of zero emission pilots and demonstration projects (2nd edition)*. Copenhagen, Denmark: Global Maritime Forum. Retrieved from https://www.globalmaritimeforum.org/content/2021/03/Mapping-of-Zero-Emission-Pilots-and-Demonstration-Projects-Second-edition.pdf

Flagships. (2021, April 7). Using river power in river boats proves the value clean waterborne operations. The Flagships Project. Retrieved from https://flagships.eu/2020/04/03/using-river-power-in-river-boats-proves-the-value-clean-waterborne-operations/

FuelCellsWorks. (2020, September 10). Norse group delivers hull of NESVIK first ferry that runs on liquid hydrogen. Montreal, Canada: Fuel Cells Works. Retrieved from https://fuelcellsworks.com/news/norse-group-delivers-hull-of-nesvik-first-ferry-that-runs-on-liquid-hydrogen/

Georgeff, E., Mao, X., Rutherford, D., & Osipova, L. (2020). *Liquid hydrogen refueling infrastructure to support a zero-emission U.S.–China container shipping corridor*. Washington, DC: International Council on Clean Transportation. Retrieved from https://theicct.org/publications/ZEV-port-infrastructure-hydrogen-2020

Global Energy Ventures. (2021). GEV scoping study delivers zero emission supply chain for green hydrogen. Claremont, Australia: Global Energy Ventures. Retrieved from https://gev.com/wp-content/uploads/2021/03/c-h2-scoping-study-delivers-green-hydrogen-supply-chain.pdf

Granath, B. (2017). Liquid hydrogen—The fuel of choice for space exploration. Washington, DC: National Aeronautics and Space Administration. Retrieved from https://www.nasa.gov/content/liquid-hydrogen-the-fuel-of-choice-for-space-exploration

Graser, A. (2019). MovingPandas: Efficient structures for movement data in Python. *GI_Forum: Journal for Geographic Information Science*, *7*(1), 54–68. https://doi.org/10.1553/giscience2019_01_s54

Hall, D., Pavlenko, N., & Lutsey, N. (2018). *Beyond road vehicles: Survey of zero-emission technology options across the transport sector*. Washington, DC: International Council on Clean Transportation. Retrieved from https://theicct.org/publications/zero-emission-beyond-road-vehicles

Hersbach, H., Bell, B., Berrisford, P., Hirahara, S., Horányi, A., Muñoz-Sabater, J., Nicolas, J., Peubey, C., Radu, R., Schepers, D., Simmons, A., Soci, C., Abdalla, S., Abellan, X., Balsamo, G., Bechtold, P., Biavati, G., Bidlot, J., Bonavita, M., … Thépaut, J. (2020). The ERA5 global reanalysis. *Quarterly Journal of the Royal Meteorological Society*, *146*(730), 1999–2049. https://doi.org/10.1002/qj.3803

Hydroville. (2017). Hydroville. Antwerp, Belgium: Hydroville. Retrieved from http://hydroville.be/en/hydroville/

Hyon. (2019). Our Projects. Oslo, Norway: Hyon. Retrieved from https://www.hyon.no/projects

HySeas III Project. (2019). The HySeas III Project. St. Andrews, Scotland: HySeas III. Retrieved from https://www.hyseas3.eu/the-project/

Jiang, J. (2020, October 23). Hydrogen-fuelled ship project secures EU funding. Singapore: Splash247. Retrieved from https://splash247.com/hydrogen-fuelled-ship-project-secures-eu-funding/

Kramer, J. A., Steen, S., & Savio, L. (2016). *Drift forces – Wingsails vs Flettner rotors*. Presented at High-Performance Marine Vehicles, Cortona, Italy. Retrieved from https://www.researchgate.net/publication/308674535_Drift_Forces_-_Wingsails_vs_Flettner_Rotors

Lele, A., & Rao, K. V. S. (2016). *Ship propulsion strategies by using wind energy.* Presented at 2016 International Conference on Emerging Technological Trends (ICETT), 1–6. https://doi.org/10.1109/ICETT.2016.7873693

Mao, X., Georgeff, E., Rutherford, D., & Osipova, L. (2021). *Repowering Chinese coastal ferries with battery-electric technology*. Washington, DC: International Council on Clean Transportation. Retrieved from https://theicct.org/publications/chinese-coastal-ferries-electric-apr2021

Mao, X., Rutherford, D., Osipova, L., & Comer, B. (2020). *Refueling assessment of a zero-emission container corridor between China and the United States: Could hydrogen replace fossil fuels?* Washington, DC: International Council on Clean Transportation. Retrieved from https://theicct.org/publications/zero-emission-container-corridor-hydrogen-2020

Maritime Executive. (2020, September 3). NYK Leads Project to Develop Hydrogen-Powered Ferry. Plantation, Florida: The Maritime Executive. Retrieved from https://www.maritime-executive.com/article/nyk-leads-project-to-develop-hydrogen-powered-ferry

Marshall, K. (2020, December 15). Norsepower announces first newbuild order with installation on bulk carrier. Helsinki, Finland: Norsepower. Retrieved from https://www.norsepower.com/post/norsepower-announces-first-newbuild-order-with-installation-on-bulk-carrier/

Minnehan, J. J., & Pratt, J. W. (2017). *Practical application limits of fuel cells and batteries for zero emission vessels* (SAND--2017-12665, 1410178). Albuquerque, NM: Sandia National Laboratories. https://doi.org/10.2172/1410178

NYK Line. (2016). NYK Super Eco Ship. Tokyo, Japan: NYK Group. Retrieved from https://www.nyk.com/english/esg/envi/ecoship/

Olmer, N., Comer, B., Roy, B., Mao, X., & Rutherford, D. (2017a). *Greenhouse gas emissions from global shipping, 2013–2015*. Washington, DC: International Council on Clean Transportation. Retrieved from https://theicct.org/publications/GHG-emissions-global-shipping-2013-2015

Olmer, N., Comer, B., Roy, B., Mao, X., & Rutherford, D. (2017b). *Greenhouse gas emissions from global shipping, 2013–2015: Detailed methodology*. Washington, DC: International Council on Clean Transportation. Retrieved from https://theicct.org/publications/GHG-emissions-global-shipping-2013-2015

Orkustofnun. (2021). Geothermal. Reykjavik, Iceland: National Energy Authority of Iceland. Retrieved from https://nea.is/geothermal/

Osnes, K. (2021). FreeCO_2ast. Fosnavåg, Norway: Havyard Group ASA. Retrieved from https://www.gceocean.no/media/2677/freeco2ast-kristian-osnes.pdf

Pearson, D. R. (2014). *The use of Flettner rotors in efficient ship design*. Presented at Influence of EEDI on Ship Design, 24–25 September, London, England. Retrieved from https://www.researchgate.net/publication/287081987_The_use_of_Flettner_rotors_in_efficient_ship_design

Seifert, J. (2012). A review of the Magnus effect in aeronautics. *Progress in Aerospace Sciences*, *55*, 17–45. https://doi.org/10.1016/j.paerosci.2012.07.001

Smith, T. W. P., Jalkanen, J. P., Anderson, B. A., Corbett, J. J., Faber, J., Hanayama, S., O'Keefee, E., Parker, S., Johanasson, L., Aldous, L., Raucci, C., Traut, M., Ettinger, S., Nelissen, D., Lee, D. S., Ng, S., Agrawal, A., Winebrake, J. J., Hoen, M., Chesworth, S., Pandey, A. (2015). *Third IMO greenhouse gas study 2014.* London, England: International Maritime Organization, p. 327. Retrieved from https://www.imo.org/en/OurWork/Environment/Pages/Greenhouse-Gas-Studies-2014.aspx

Talluri, L., Nalianda, D. K., & Giuliani, E. (2018). Techno economic and environmental assessment of Flettner rotors for marine propulsion. *Ocean Engineering*, *154*, 1–15. https://doi.org/10.1016/j.oceaneng.2018.02.020

Thouault, N., Breitsamter, C., Seifert, J., Badalamenti, C., & Prince, S. A. (2012). Numerical analysis of a rotating cylinder with spanwise discs. *AIAA Journal, 50*(2). https://doi.org/10.2514/1.J050856

Tillig, F., & Ringsberg, J. W. (2019). A 4 DOF simulation model developed for fuel consumption prediction of ships at sea. *Ships and Offshore Structures*, *14*(sup1), 112–120. https://doi.org/10.1080/17445302.2018.1559912

Tillig, F., & Ringsberg, J. W. (2020). Design, operation and analysis of wind-assisted cargo ships. *Ocean Engineering*, *211*, 107603. https://doi.org/10.1016/j.oceaneng.2020.107603

Tillig, F., Ringsberg, J. W., Mao, W., & Ramne, B. (2018). Analysis of uncertainties in the prediction of ships' fuel consumption – from early design to operation conditions. *Ships and Offshore Structures*, *13*(sup1), 13–24. https://doi.org/10.1080/17445302.2018.1425519

Ulstein. (2021, November 2). Zero-emission operations in offshore construction market. Ulsteinvik, Norway: Ulstein Group. Retrieved from https://ulstein.com/news/2019/zero-emission-operations-in-offshore-construction-market

U.S. Department of Energy. (2014). Fuel Cell Technologies Office - Hydrogen Delivery. 2.

Wallace, J. M., & Hobbs, P. V. (2006). *Atmospheric science: An introductory survey* (2nd ed). Cambridge, Massachusetts: Academic Press.

Water-Go-Round. (2021). Water-Go-Round. Retrieved from https://watergoround.com/

Wilhelmsen. (2020, December 17). Wilhelmsen's Topeka hydrogen project awarded NOK 219 million. Lysaker, Norway: Wilhelmsen. Retrieved from https://www.wilhelmsen.com/media-news-and-events/press-releases/2020/wilhelmsens-topeka-hydrogen-project-awarded-nok-219-million/

Zhou, Y., Pavlenko, N., Rutherford, D., Osipova, L., & Comer, B. (2020). *The potential of liquid biofuels in reducing ship emissions*. Washington, DC: International Council on Clean Transportation. Retrieved from https://theicct.org/publications/marine-biofuels-sept2020

APPENDIX A. WEATHER DATA DETAILS

Data characterizing the near-surface weather characteristics came from 2 m to 10 m in altitude above ground level in the specified geographical domains. The chosen surface-level variables were temperature, dewpoint temperature, surface pressure, and horizontal east–west (u) and north–south (v) wind components. Data characterizing the atmospheric boundary layer conditions from 0 to 100+ m above ground level were taken from vertical model levels at each latitude–longitude grid point. The appropriate conversions from the model coordinates to altitude were made assuming conventional balance approximations in the vertical axis (Wallace & Hobbs, 2006). The chosen atmospheric boundary layer variables were temperature, relative humidity, geopotential height, and horizontal east–west (u) and north–south (v) wind components. The nominal values of the atmospheric pressure for each model level were recorded.

Each weather data output time was assumed to be representative of a one-hour window centered on the analysis time (i.e., analysis time +/- 0.5 hr) coinciding with the hourly AIS reports for each vessel position. The weather analysis land–ocean mask variable was used to identify ocean areas having the majority of the contained area in the model grid box occupied by water (>50%). The weather data were then attributed to each vessel position using a nearest neighbor approach in space. With the index of the nearest neighbor weather model data grid point over ocean, surface and above-surface weather variables could be queried at once.

Vertical profiles of wind were computed by concatenating the near-surface winds from 10 m up through approximately 1.5 km in altitude and using cubic-spline interpolation. The east–west (zonal) and north–south (meridional) components from the weather model were translated into true wind speed and direction (i.e., the compass direction that the wind originates from); the true wind could be resampled at any altitude of choice thereafter. Local density at nonstandard altitudes was found by first linearly interpolating temperature to the desired height from the near-surface reference level (altitude = 2 m) up to approximately 1.5 km in altitude. The exponential decrease in atmospheric pressure above a given location was next approximated using the resulting mean temperature in each layer and the hypsometric equation (Wallace & Hobbs, 2006). Then the density, a function of local pressure, temperature, and moisture, was calculated using the equation of state. Note that the calculation of density accounts for the presence of water vapor, as it can lead to local decreases in pressure and therefore density.

APPENDIX B. UPDATED METHODS FOR ESTIMATING ENERGY SAVINGS FROM ROTOR SAILS

We made several updates to the methodology of Comer et al. (2019), primarily focused on refining the equations related to aerodynamic force. Comer et al. (2019) used static lift and drag exchange coefficients following Lele and Rao (2016) and Craft et al. (2012); importantly, static lift and drag coefficients were not assumed to be dependent on the SR, which Comer et al. (2019) previously assumed to be constant at 5.0. Subsequent research has shown that lift and drag coefficients are strongly sensitive to the assumption of SR. Tillig and Ringsberg (2020) proposed adaptations to the conventional approach whereby lift (C_L), drag (C_D), and power (C_P) coefficients are variable with respect to SR, and we followed their revised approach here. The parameterizations for each coefficient follow a fifth-order polynomial form as shown below (Bordogna et al., 2020; Da-Qing et al., 2012; Kramer et al., 2016):

$$C_L = -0.0046 \times SR^5 + 0.1145 \times SR^4 - 0.9817 \times SR^3 + 3.1309 \times SR^2 - 0.1039 \times SR$$

$$C^D = -0.0017 \times SR^5 + 0.0464 \times SR^4 - 0.4424 \times SR^3 + 1.7243 \times SR^2 - 1.641 \times SR + 0.6375$$

$$C^P = 0.0001 \times SR^5 - 0.0004 \times SR^4 + 0.0143 \times SR^3 - 0.0168 \times SR^2 + 0.0234 \times SR$$

The parameterizations above from Tillig and Ringsberg (2020) assume a rotor sail AR of 6 from Talluri et al. (2018). To ensure that our results are consistent with the assumptions that were previously established, we adopted the convention of AR = 6 for this study by assuming rotor sail dimensions of 24 m x 4 m in height and diameter, respectively.

Next, we considered the potential influence of adding rotor endplates, which can both reduce overall drag by suppressing wake vortices that commonly develop on the edges of airfoils (Badalamenti & Prince, 2008) and boost lift by more efficiently focusing inflow on the surface of the rotor sail. In other words, installing endplates increases lift-to-drag ratio. We assumed that the endplates' diameter was 1.5x larger than the diameter of the rotor sail, consistent with Badalamenti and Prince (2008), and we modified the lift and drag coefficients according to the following piecewise expressions for endplate correction factors with dependence on SR:

Correction to C_L

$$\textit{Correction to } C_L \begin{cases} SR < 2.0 \mid \textit{None} \\ SR = 2.0 \mid 0.25 \\ SR \geq 3.0 \mid 0.50 \end{cases}$$

Correction to C_D

$$\textit{Correction to } C_D \begin{cases} SR < 2.0 \mid \text{None} \\ SR = 2.0 \mid 0.10 \\ SR \geq 3.0 \mid 0.20 \end{cases}$$

Furthermore, we assumed that the addition of endplates did not contribute significantly to the power required to spin each rotor sail. Thus, we did not make any modification to C_P to account for the presence of the endplates. We acknowledge that the addition of mass at the top of the rotor sail would theoretically lead to increases in power required to operate the rotor (Thouault et al., 2010), but for simplicity we assume that this increase is negligible.

We conducted a supplementary analysis and determined that for oceanic locations within our domains of interest, the wind speed can vary by at least 2.0 m s^{-1} within the

lowest 30 to 50 m of the atmosphere (i.e., as a function of altitude), on average. As an update to the previous Comer et al. (2019) methodology, which assumed a constant wind speed along the height of the rotor, we computed net power savings for this study assuming different wind speeds at *N* different heights (6 m increments) between the bottom and top of the rotor sail (reference Figure 4 from Tillig and Ringsberg, 2019). For example, assuming the bottom of the rotor sail was situated on the vessel's deck at 10 m above the water surface, *N* = 4 and the theoretical heights for wind velocity calculations would be 13, 19, 25, and 31 m.

$$P_{net} = P_{gen} - P_{cons} = \sum_{i=1}^{N} C_T \frac{\rho A_{proj}}{2N} AWS^2 v_s - C_P \frac{\rho A_{proj}}{2N} AWS^3$$

$$C_T = C_L \sin(AWA) - C_D \cos(AWA)$$

In the equations above, P_{net}, P_{gen}, and P_{cons} are the net power, power generated, and power consumed by each rotor sail, respectively; C_T and C_P are the thrust and rotor power coefficients; ρ is air density assuming that the local atmosphere is made up of dry air and water vapor; A_{proj} is the total projected surface area exposed to the apparent wind for *N* vertical partitions of the rotor sail; *AWS* is the apparent wind speed; *AWA* is the apparent wind angle; and v_s is the vessel speed. Comer et al. (2019) used the entire surface area of the rotor for calculating the power required to spin each rotor sail, whereas in the current study, we ran calculations assuming the projected surface area of the rotor sail was affected (i.e., accounting for a reduction in the area term by a factor of π), following the approach of Tillig and Ringsberg (2019). Lastly, we applied a propulsion efficiency factor of 0.75 to P_{net} to account for general system losses in power from rotor sails to the vessel's propellor power output (Lele & Rao, 2016).

Tillig and Ringsberg (2019, 2020) examined aerodynamic performance of the rotor with hydrodynamic resistance factors such as added drift, rudder drag, and sway from wave action; the added hydrodynamic resistance offsets some of the energy savings generated by the rotor sails. Instead of modeling the hydrodynamic resistance for each factor, we took a simplified approach. As mentioned earlier, the SAVE model includes a weather-adjustment factor that adds 10% to main engine power demand near shore (≤5 nm) and 15% away from shore (>5 nm) to overcome resistance from weather and waves. Colocated meteorological and oceanographic observations show that wind and waves are considerably more intense farther from the coast (Ahsbahs et al., 2017).We adopted this approach because we did not have complete ship design specifications such as hull design and superstructure dimensions or reliable ocean wave spectra available for our reporting, and because the fuel consumption and therefore energy use estimates from the SAVE model correlate well with the approach of the Fourth IMO GHG Study, which itself matches well with reported fuel consumption from the EU Monitoring Reporting and Verification Scheme, as explained by Faber et al. (2020).

We conducted a sensitivity analysis of the net power-saving potential using rotor sails with respect to the assumed size (i.e., projected rotor sail surface area) as well as to the assumed SR. Also, this study employed an updated version of the numerical weather model used to supply atmospheric conditions at each vessel position and time.